Chemistry Europe
European Chemical Societies Publishing

Carbon Pathways, Sodium-Sulphur Promotion and Identification of Iron Carbides in Iron-based Fischer-Tropsch Synthesis

Pasi P. Paalanen[a] and Bert M. Weckhuysen*[a]

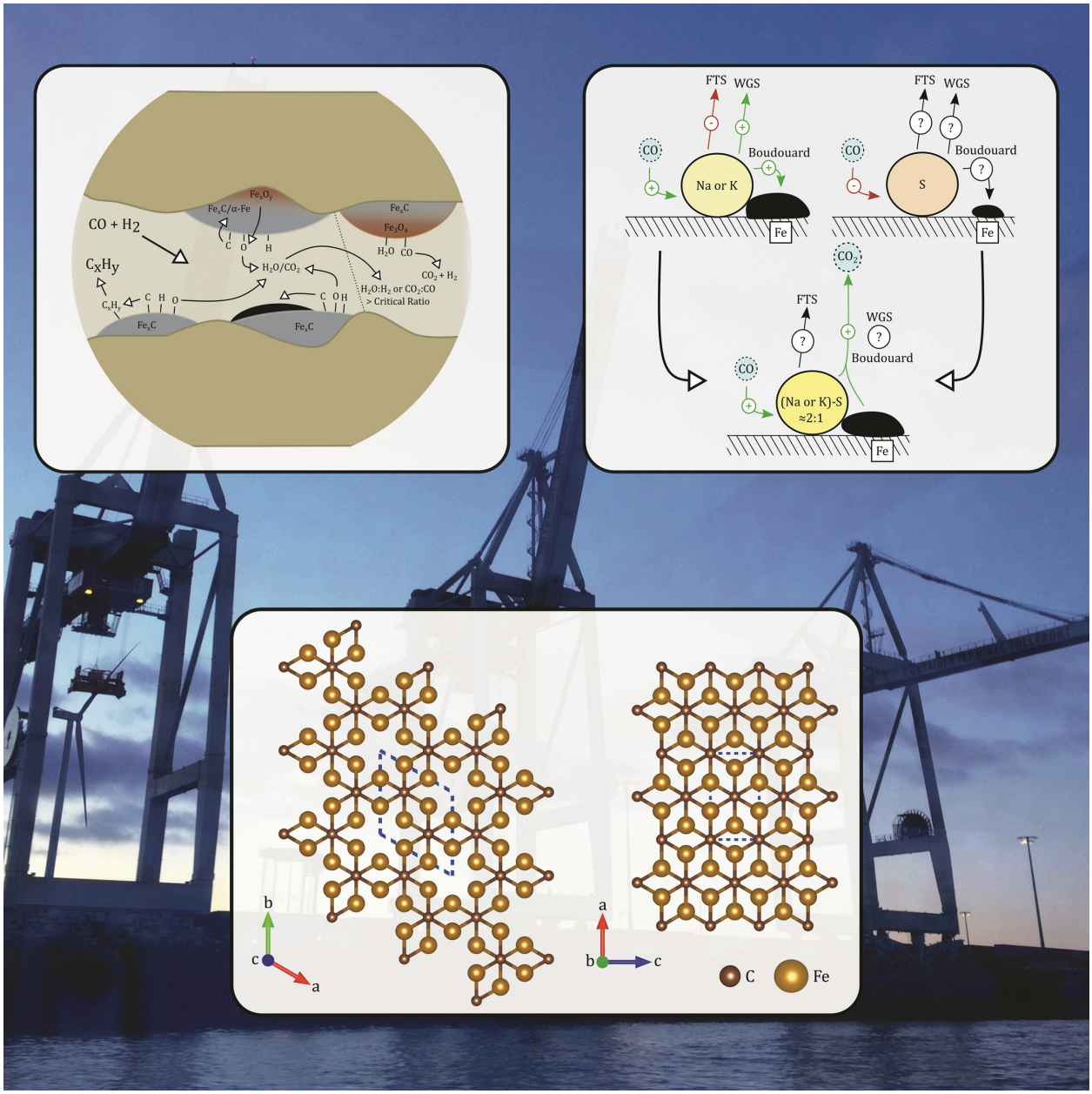

Fisher-Tropsch Synthesis (FTS) is industrially used for converting a carbon-containing feedstock, such as coal, natural gas, biomass, and municipal waste, via the production of synthesis gas (a mixture of $CO+H_2$) into hydrocarbons. This review article focuses on Fe-based FTS catalysis, thereby focusing on the process conditions available for steering the various carbon pathways from input CO and their associated reactions. We will also discuss the effects of alkali-sulphur chemical promotion and the identification of the FTS reaction active Fe carbides, which are assigned with precise crystal structures and nomenclature. Each observed Fe carbide crystal structure is further assigned with corresponding Mössbauer Absorption Spectroscopy (MAS) hyperfine fields. The expected formation temperatures and experimental conditions for the identified Fe carbides encountered in FTS research, namely ε-Fe_3C, η-Fe_2C, χ-Fe_5C_2, θ-Fe_3C and θ-Fe_7C_3, are reviewed.

1. Introduction

The Fischer-Tropsch Synthesis (FTS) reaction can be used to convert a $CO+H_2$ gas mixture (i.e., synthesis gas or syngas) produced from a carbon-containing feedstock into a mixture of hydrocarbons. The FTS reaction can be idealized as (**Reaction 1**),

$$CO + 2\ H_2 \rightarrow -(CH_2) - + H_2O \quad (1)$$

where the hydrocarbons are polymerized from $-(CH_2)-$ units and O atom from CO is removed as H_2O.[1]

In an industrial setting, the application of FTS reaction becomes Fischer-Tropsch Process (FTP) where i) a carbon-containing feedstock is converted into syngas, ii) a FTS reaction is utilized and iii) the FTS reaction produced hydrocarbon mixture (i.e., synthesis crude or syncrude) is refined into hydrocarbon products (Figure 1).[2,3]

The complete FTP can be labelled after the feedstock: Biomass-to-Liquids (BTL), Coal-to-Liquids (CTL), Gas-to-Liquids (GTL) and Waste-to-Liquids (WTL). The effective H:C ratio of the syngas is the actual ratio of elemental H:C available for the FTS reaction after all of the heteroatoms (N, O, S) in the feedstock are hydrogenated and subsequently removed during a syngas cleaning step (Table 1).[4,5] The used feedstock dependent CO_2 footprints are in the order: GTL < WTL < CTL < BTL with an inverse relation to the effective H:C ratio (Table 1). That is, the increase in the CO_2 footprint due to input feedstock fundamentally comes from the necessity of adding more H to the system for satisfying the required FTS reaction stoichiometry of 4:1 H:C.[4,5]

Despite that the syngas production step can have a significant impact,[4,6] it is not the only step affecting the FTP's CO_2 footprint. Each process step, from feedstock to refined hydrocarbon products, should be optimized by the Green Chemistry principles: *avoiding waste*, *maximizing atom economy*, *increasing energy efficiency and designing less hazardous chemical syntheses*.[4] In other words, from each process input CO molecule maximum amount elemental C should end up to the hydrocarbon products with minimum energy used, and waste products formed.

The C atom efficiencies for the total FTP from feedstock into hydrocarbon products currently stand at ~75% for GTL,[4] and ~28–34% for CTL.[4,5] For comparison, in crude oil refineries the C efficiency is estimated to be ~89%.[4] The production of purified syngas accounts for ~30–50% of the capital costs for GTL- and ~60–70% for CTL-based processes.[2,3] The expensive syngas should be turned into hydrocarbon products as efficiently as possible also from the viewpoint of economic viability of the FTP.

To maximize the FTP C efficiency and adherence to Green Chemistry Principles, the syngas conversion process to syncrude with the FTS reaction still needs improvements. The main ways to achieve this is to alter catalyst compositions and reaction conditions for the FTS reaction.

With varying the catalyst material compositions (e.g., active d-block metal, support material and structural and/or chemical promoters) the catalysts behaviour can be modified.[1,7,16,17,8–15] General requirements for an industrially good FTS reaction catalyst material are: i) sufficient activity towards FTS reaction, ii) high selectivity for converting the input CO only to the desired hydrocarbons and iii) mechanical and catalytical stability.[4] Despite most of the d-block transition metals being somewhat active towards the FTS reaction,[1,18,19] catalysts based on Fe and Co are the most suitable ones for FTS reaction applications. Consequently, only Fe- and Co-based catalysts have been applied on a large scale in industry.[1,4]

The reaction conditions (e.g., reaction temperature, input feed H_2:CO ratio and pressure) have a significant effect on which hydrocarbon products are formed. In the currently operational industrial Fischer-Tropsch facilities, either Low-temperature Fischer-Tropsch (200–250 °C, LTFT) or High-temperature Fischer-Tropsch (320–375 °C, HTFT) have been used with reaction pressures of 15–60 bar.[4]

Fe-based catalyst materials have been used on both LTFT and HTFT, while Co has only been used for LTFT. Fe-HTFT is best suited for producing syncrude with short-chained unsaturated hydrocarbons, while the low temperature Fe- or Co-LTFT favours production of syncrude with long-chained saturated hydrocarbons.[4] In terms of catalyst stabilities, Fe-based FTS catalyst materials can be stable up to ~4 months for LTFT and ~1.5 months for HTFT, while Co-based LTFT catalysts can be used for up to a couple of years.[4]

[a] P. P. Paalanen, Prof. B. M. Weckhuysen
Inorganic Chemistry and Catalysis group, Debye Institute of Nanomaterials Science
Utrecht University
Universiteitsweg 99, postCode/>3584 CG Utrecht (The Netherlands)
E-mail: b.m.weckhuysen@uu.nl

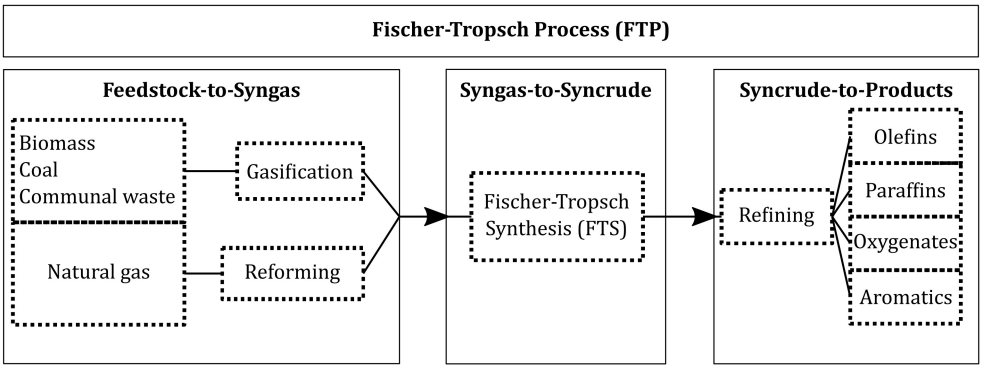

Figure 1. The overall Fischer-Tropsch Process (FTP) for converting carbon containing feedstocks into various product hydrocarbons utilizing the Fischer-Tropsch Synthesis (FTS) reaction in the process.

Table 1. Estimated CO_2 footprint for the total Fischer-Tropsch Process (FTP) as depending only on the process input feedstock. The Table is modified from reference [4].

Feedstock	Elemental Analysis [wt-%]					H:C (elemental ratio)		CO_2 footprint due to feed[a] (CO_2:Hydrocarbons kg:kg)
	C	H	N	S	O	Nominal	Effective	
Natural gas[b]	74.9	25.1	0	<0.1	0	4.00	4.00	0.00
Waste[c]	53.3	8.2	4.9	0.1	33.5	1.83	0.65	3.96
Coal[d]	75.7	5.0	1.2	1.0	17.1	0.80	0.40	4.80
Biomass[e]	50.1	6.1	0.9	0.1	42.8	1.45	0.12	5.75

[a] Based in ideal Fischer-Tropsch Synthesis (FTS) reaction i.e. [Eq. (1)] $CO + 2\,H_2 \rightarrow -(CH_2)- + H_2O$. CO_2 footprint estimated from carbon efficiency using CO_2 equivalent. [b] Dry natural gas with all the hydrocarbons removed. [c] Municipal waste. [d] Mean values over various coal types. [e] Switchgrass.

This article reviews a selection of topical aspects on Fe-based FTS catalysis. The first major topic of this review is to discuss and define the possible reaction pathways for C atoms from input CO in the FTS reaction. How the reaction conditions and some aspects of catalyst composition affect these "C pathways", catalyst phase changes and deactivation, and thus the overall C efficiency towards hydrocarbons are then further reviewed with a clear focus on Fe-based FTS reaction chemistry. The effects from Na–S chemical promotion,[20–24] are discussed as well. As a second major topic of this review, the identification and formation conditions of the various Fe carbides encountered in the Fe-based FTS reaction are discussed. Exact crystal structures and Mössbauer Absorption Spectroscopy (MAS) hyperfine fields are assigned for the identified Fe carbides. This task is performed in order to clarify the often imprecise and unclear nomenclature used in FTS literature for the different Fe carbide phases. The clarified Fe carbide nomenclature will help future, and in interpreting the past, studies to assign more definite catalytic properties and effects for the Fe carbide phases in the FTS reaction.

The topic of Fe-based catalyst synthesis is excluded from this review. Discussion of catalyst synthesis effects on FTS reaction can be found from e.g. review article by Torres Galvis and de Jong.[7]

2. Overview of Fischer-Tropsch Synthesis

2.1. Reactions

The exothermic main chemical reaction in the FTS is the conversion of the input H_2:CO gas mixture into various hydrocarbons and the side-product H_2O,[25,26]

Pasi P. Paalanen obtained his BSc degree on Physical Chemistry from the University of Jyväskylä (Finland) in 2011 After this, he completed his MSc degree on Nanomaterials Science at Utrecht University (the Netherlands) in 2013, where he also continued his PhD work focusing on the Fe-based Fischer-Tropsch Synthesis reaction and its spectroscopic characterization.

Bert M. Weckhuysen obtained his PhD degree from K.U.Leuven (Belgium) in 1995. After postdoctoral stays at Lehigh University (PA, USA) and Texas A&M University (TX, USA) he became in 2000 Full Professor at Utrecht University (the Netherlands). His research focuses on the development and use of in-situ and operando spectroscopy for studying solid catalysts under realistic reaction conditions at different length scales.

$$n\ CO + (2n+1)\ H_2 \rightleftharpoons C_nH_{2n+2} + n\ H_2O \quad (2)$$

$$n\ CO + 2n\ H_2 \rightleftharpoons C_nH_{2n} + n\ H_2O \quad (3)$$

where **Reaction 2** refers to formation of paraffins (i.e., saturated hydrocarbons) and **Reaction 3** refers to formation of olefins (i.e., unsaturated hydrocarbons). The olefins formed as the FTS reaction's primary products may re-adsorb on the catalyst material and be hydrogenated into paraffins via secondary reactions.[26,27]

Both CO and H_2 adsorb dissociatively under the FTS reaction conditions giving C, O and H atoms adsorbed on the Fe phases' surface. H and C atoms then recombine to form -CH_2- units which polymerize to hydrocarbon chains, via the so-called "surface carbide mechanism".[25,26,28] Preferably, the O atoms from the CO dissociation recombine with H atoms and desorb as a H_2O molecule. If H_2 is unavailable, as can be the case with low H_2:CO ratio syngas,[5] the adsorbed O atom from the CO dissociation may react with an another CO molecule and be removed as CO_2.[1,28,29] Several mechanisms for the FTS reaction have been proposed to explain the variety of hydrocarbon products and their derivatives.[1,25,28,30] Within this article for the sake of simplicity, their existence is acknowledged, but only the surface carbide mechanism is considered to be active.

The formation of oxygenate derivatives of hydrocarbons (mainly alcohols) can be taken as a side-reaction, as their contribution to the overall FTS reaction products is usually low.[1,4,31] Saturated alcohols form in the FTS reaction according to reaction equation:[26]

$$n\ CO + 2n\ H_2 \rightleftharpoons C_nH_{2n+1}OH + (n-1)\ H_2O \quad (4)$$

Besides the **Reaction 4** for exothermic formation of alcohol oxygenates, also some water soluble carboxylic acids and aldehydes may form in the FTS reaction.[1,4,31] The generic reaction equations for the carboxylic acid and aldehyde formation are omitted here, but can be found e.g. as presented by Dry.[1]

The Water-Gas Shift (WGS) reaction is used on an industrial scale in the production of H_2.[32,33] It follows the reaction equation:

$$CO + H_2O \rightleftharpoons CO_2 + H_2 \quad (5)$$

The WGS reaction is not usually active for Co-based FTS reaction catalyst materials, but can be active under the FTS reaction conditions for Fe-based catalysts (**Reaction 5**).[3,25,26,34–36] With increasing reaction temperature, the WGS reaction equilibrium shifts towards the formation of the reactants CO and H_2O (i.e., it is an exothermic reaction). If the reaction is kinetically limited i.e. CO + H_2O partial pressures are above the equilibrium expectations, the total forward reaction may benefit from an increased reaction temperature.[33,37] In the presence of sufficient amounts of CO_2 and H_2, the reverse WGS reaction can also take place forming CO and H_2O.[29,31,38–40] In the industrial application of the WGS reaction, a Cu/ZnO/Al_2O_3 catalyst material is used for ~210–240 °C and a Fe_3O_4/Cr_2O_3 catalyst for ~310–450 °C reaction temperatures.[32,33,37] For both high and low WGS reaction temperatures, the reaction proceeds with an oxidic active phase unable of CO dissociation.[32,33] This is unlike as in the FTS reaction where CO is dissociatively adsorbed by Fe carbides.

The Boudouard reaction is an unwanted reaction pathway under the FTS reaction conditions causing formation of inactive carbon species ("coke") on the catalyst:[41]

$$2\ CO \rightleftharpoons C + CO_2 \quad (6)$$

The Boudouard reaction (i.e., CO disproportionation) deposits adsorbed carbon species on the catalyst, while releasing CO_2 (**Reaction 6**). When raising the FTS reaction temperature from LTFT at ~225 °C to HTFT conditions at ~345 °C, the rate of carbon deposition becomes significant for Fe-based FTS catalyst materials at $\gtrsim$ 300 °C.[1,42–44] The Boudouard reaction becomes a major reaction consuming CO, if the CO is exposed to Fe at temperatures $\geq$ 400 °C.[45,46] The generic types of inactive carbon formed are either encapsulating carbon over the Fe phases if only CO is present or filamentous carbon if both CO and H_2 are available.[47–49]

Small amounts of added H_2, or H_2O converted to H_2 via the WGS reaction, can increase the carbon deposition rate from the Boudouard reaction.[1,43,50,51] H_2 removes the adsorbed and catalyst surface sites blocking O atoms from the CO dissociation as H_2O. The O removal is done with H_2 to H_2O more efficiently than with CO to CO_2. The improved O removal probably increases the rate at which CO molecules can adsorb and dissociate on the surfaces of (near-)zerovalent Fe phases (i.e. α-Fe or Fe_xC).[29,52] However, the increased carbon deposition only takes place with small amounts of added H_2 to input CO. If higher H_2:CO ratios ($\gtrsim$ 5:1) with above ~15–20 bar total reaction syngas pressure are used, the carbon deposition can be decreased during the FTS reaction in relation to the hydrocarbon formation.[1,53]

2.2. Fe Phase Changes

Several possible Fe phase changes take place on a Fe-based catalyst material when moving from the as-synthesized catalyst to a catalyst under FTS reaction conditions and, possibly, to a deactivated catalyst material. The generic Fe phase changes for a Fe-based catalyst follow the following order:[1,25,31]

Initial Catalyst (Fe oxide) ⟹ **Reduced Catalyst** (Metallic Fe) ⟹ **Active Catalyst** (Fe carbide)

The initial FTS reaction catalyst material is commonly in a form of a Fe oxide, mainly either as α-Fe_2O_3 (hematite), γ-Fe_2O_3 (maghemite) or Fe_3O_4 (magnetite).[25] The Fe oxides are not active for the hydrocarbon-forming FTS reactions (**Reaction 2** and **Reaction 3**),[54–56] and are commonly reduced to α-Fe (metallic Fe) prior to starting the FTS reaction. Upon exposure to H_2:CO in the FTS reaction, the α-Fe then readily reacts to form various Fe carbide phases (Fe_xC, $x = 2$–3).[30,57–61] Alterna-

tively, the Fe oxides can also be exposed directly to the FTS reaction conditions, i.e. to a H_2:CO atmosphere. In this occasion the FTS active Fe carbides form simultaneously with the Fe oxide reduction to α-Fe.[27,46,62–66]

The reaction equations for reducing Fe oxides to metallic α-Fe with either H_2 or CO are:[25,26,67]

$$Fe_xO_y + y\ H_2 \rightleftharpoons \times Fe + y\ H_2O \tag{7}$$

$$Fe_xO_y + y\ CO \rightleftharpoons \times Fe + y\ CO_2 \quad 500\,^\circ C \tag{8}$$

$$Fe_xO_y + (y+2)\ CO \rightleftharpoons Fe_xC + (y+1)\ CO_2 \quad 500\,^\circ C \tag{9}$$

Fe oxide reduction with H_2 leads to formation of pure metallic α-Fe (**Reaction 7**). In general, a H_2 reduction temperature of $\gtrsim 350\,^\circ C$ is required, with adequate reaction time, for reducing Fe_xO_y to α-Fe.[67] The most stable Fe_xC phase (namely θ-Fe3C) decomposes between 500–600 °C into α-Fe and carbon species.[68–71] Thus, only α-Fe is observed as the CO reduction product $\gtrsim 500\,^\circ C$ (**Reaction 8**).[67,70] With CO (or H_2:CO) reduction temperatures of $\lesssim 500\,^\circ C$, Fe_xC phases are stable and can form, i.e. the Fe oxides are reduced to α-Fe and simultaneously carburized (**Reaction 9**).[57,68,70]

Furthermore, the H_2 reduction pathway for the Fe oxides is dependent on the used temperature:[67]

$$Fe_2O_3 \rightarrow Fe_3O_4 \rightarrow Fe^0 \quad 570\,^\circ C \tag{10}$$

$$Fe_2O_3 \rightarrow Fe_3O_4 \rightarrow Fe_xO \rightarrow Fe^0 \quad 570\,^\circ C \tag{11}$$

With H_2 reduction temperatures above 570 °C (**Reaction 11**), an intermediate Fe_xO (wüstite) phase appears, which is absent if the reduction is done $\lesssim 570\,^\circ C$ (**Reaction 10**).[67] Experimentally, however, the Fe_xO phase can be stabilized also at lower temperatures $\lesssim 570\,^\circ C$ by a strong interaction between the Fe oxide with other oxides (e.g., SiO_2) or by addition of alkali (e.g., K).[67,72] The Fe_xO phase is an intermediate also if the reduction is done with CO instead of H_2, with a reduction temperature $\gtrsim 570\,^\circ C$.[67]

At sufficiently high reduction temperatures, Fe_3O_4 may go through an undesired solid-state reaction with the support or the structural promoter inert oxide.[3,73] As an example, the formation of $FeAl_2O_4$ (i.e., Fe aluminate) with a Fe/γ-Al_2O_3 catalyst at temperatures at ~450–470 °C, can take place.[74] Such solid-state reactions are undesirable as Fe in the $FeAl_2O_3$ compound stays in the oxidized, inactive ionic state for the FTS reaction.[3,73]

The FTS reaction active Fe_xC phases form in the presence of CO from reduced α-Fe (**Reaction 12**):

$$xz\ Fe + 2z\ CO \rightarrow z\ Fe_xC + z\ CO_2 \tag{12}$$

where $x = 2–3$ and $z = 2x–3$. If H_2 is also present during the carburization reaction, then the O atoms from CO dissociation may also be removed as H_2O instead of CO_2, as was discussed earlier in this article.

2.3. Catalyst Deactivation

The primary pathways for Fe-based catalyst deactivation in the FTS reaction are:[1]

i) **Fe phase changes** – conversion of the FTS reaction active Fe_xC into inactive Fe_3O_4,
ii) **Metal carbide sintering** – loss of active Fe_xC surface area due to increasing Fe particle size,
iii) **Catalyst fouling** – deposition of inactive carbon on the catalyst material, and
iv) **Chemical poisoning** – deposition of chemical compounds of e.g. S, Cl, Br, Pb or Sn, on the Fe_xC surface.

The conversion of Fe_xC phases into Fe_3O_4 takes place if either of the H_2O:H_2 or CO_2:CO ratios are above critical molar ratios.[1,32,33,56,62,75–77] In general, H_2O is more potent Fe oxidant than CO_2.[32,62,77] When moving along a fixed bed reactor towards the FTS reactor outlet,[64,78] or towards the inner core of the Fe-based catalyst material particle,[56] the reducing H_2:CO mixture is progressively converted into H_2O and CO_2. Due to the increasing H_2O and CO_2 concentrations, the oxidation potential towards forming Fe_3O_4 from Fe_xC increases.[1,56,75,76] Up to around 100–200 μm depth from the particle surface, the Fe-based catalyst particle might remain under reductive environment at FTS reaction conditions. For depths beyond > 200–400 μm from the particle surface, the environment may become oxidative and Fe_xC oxidation to Fe_3O_4 can take over.[56]

As Fe_3O_4 is active for the WGS, but not for the FTS reaction,[1,32,33] with sufficient reaction temperature (> 310 °C), the catalyst may become a bifunctional catalyst where the Fe_xC catalyst partially re-oxidizes to Fe_3O_4, which works as a WGS catalyst and the remaining Fe_xC part acts as the FTS reaction catalyst. At lower (< 310 °C) temperatures, the Fe_3O_4 phase is a less efficient WGS reaction catalyst.[32,33]

The loss of active Fe surface area via Fe particle growth, i.e. sintering, can cause a loss in the number of available active Fe surface sites towards catalytic reactions. This in turn causes lost activity towards the FTS reaction. Deposition of the inactive carbon, i.e. fouling, takes place in the presence of CO or H_2:CO, causing gradually lost FTS reaction activity as the active Fe sites become harder to access for the reactants.[1] Excessive inactive carbon deposition via the Boudouard reaction (**Reaction 6**) and/or carbon filament growth causes fragmentation of the, especially bulk, Fe-based catalyst materials into a fine powder.[1,3,4,76,79] The carbon deposition relates to metal carbide sintering in a two-fold manner: i) initially the availability of the FTS reaction active Fe_xC sites may increase due to catalyst fragmentation into smaller Fe particles exposing new active Fe_xC surface sites. However, ii) after a longer Time-on-Stream (ToS) the Fe tends to sinter into larger Fe particles, thereby resulting in a loss of the available Fe_xC surface area.[25,80]

The fragmentation of the Fe-based FTS reaction catalyst materials by carbon deposition and growth is a major issue for their industrial application.[79] The catalyst fragments cause clogging downstream from the FTS reactor and the fragments also need to be separated from the liquid/wax hydrocarbon products.[1,3,4,79] If a Fe-based FTS reaction catalyst material is deactivated by carbon deposition but without fragmentation, it

can be regenerated with H_2 reduction at temperatures >350 °C by hydrogenating and removing the carbon deposits.[1] However, if the catalyst material has fragmented, the resulting fine Fe powder still needs to be dealt with to avoid the related issues.[1,3,4,79] In this case, the simple H_2 regeneration is an insufficient method for increasing the Fe catalyst's life-time.

Deposition of chemical compounds on the Fe phases can decrease their reactivity under FTS reaction conditions. Commonly, the addition of electropositive compounds as chemical promoters (e.g., K or Na compounds) can have a beneficial effect on the hydrocarbons-forming FTS reaction.[1,34,36,81] While deposition of electronegative compounds, most commonly S-containing compounds, have a deactivating effect decreasing CO conversion and thus FTS reaction activity.[1,22,82–84]

Work function describes the minimum energy that is required to remove an electron from a chemical compound's highest occupied energy level (the Fermi level).[85] In general, lower the work function, the easier for a chemical phase is to donate electrons towards an adsorbate causing it to react. Within context of current discussion, the electronegative compounds increase the α-Fe/Fe_xC surface's work function, thereby lowering its reactivity and ability to adsorb and dissociate H_2 and CO.[86–89] Deactivation of Fe phases with S-containing compounds is not only via the mentioned electronic effects, but also via geometric effects; i.e., Fe_xC surface site dependent effects.[87,88,90] These electron donation, work function and geometric effects are discussed in more detail later in the text.

Thus, to summarize the discussion so far, a C atom from input CO has five distinct pathways to react under FTS reaction conditions when a Fe-based catalyst material is used (Figure 2):

i) with α-Fe to form Fe_xC phases (**Reaction 12**),
ii) with H to form hydrocarbons (**Reactions 2** and **3**),
iii) with C to form inactive carbon (**Reaction 6**),
iv) as CO to form CO_2 via Fe_xO_y reduction (**Reaction 9**),
v) as CO to form CO_2 via WGS reaction (**Reaction 5**).

The O from CO dissociation is removed as H_2O or CO_2, possibly gradually transforming the FTS reaction atmosphere, from reductive/carburizing H_2:CO towards oxidative H_2O- and/or CO_2-rich conditions. Under the oxidative atmosphere, FTS reaction active Fe_xC may re-oxidize to Fe_3O_4, a phase which can catalyze the WGS reaction. The reverse WGS reaction in turn may convert CO_2 back to CO. Ideally, only pathway 2) should be active with all the O atoms preferably removed as H_2O. This in order to achieve the ideal FTS reaction carbon efficiency from the input H_2:CO (**Reaction 1**).[5]

3. Process Conditions

The main FTS reaction process parameters for controlling the formed hydrocarbon products and the C reaction pathways are i) reaction temperature, ii) input H_2:CO ratio and iii) the used gas space velocity. The effect of total reaction pressure is less straightforward for Fe-based FTS reaction catalysts, based on the open literature available. It is important to note that the CO conversion level directly by itself does not significantly affect the hydrocarbon selectivities.[34,91] The discussion on FTS reaction process conditions is held with assumption of powdered catalysts, i.e. effects arising from e.g. shaped extrudates are not discussed.

3.1. Reaction Temperature

Reaction temperature has the effect of decreasing the α-value (i.e., the hydrocarbon chain length).[1,8,27,91,92] The reaction temperature's effect is more complex and unclear with respect

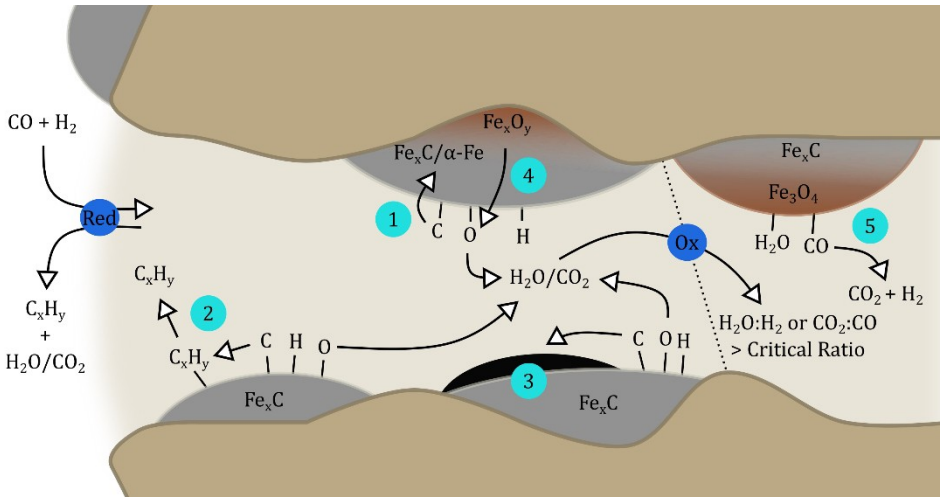

Figure 2. A simplified summary of reaction pathways for C atoms from input CO in a Fe-based Fischer-Tropsch Synthesis (FTS) reaction catalyst particle. The input CO + H_2 gives originally a reductive environment (*Red*). For *C from CO dissociation* the pathways to react are: (1) with α-Fe to form Fe_xC, (2) with H to form hydrocarbons, (3) with C to form inactive carbon. *Without CO dissociation*: C pathway (4) may reduce Fe_xO_y to α-Fe while releasing CO_2. Removal of O atoms from CO as H_2O or CO_2 gradually leads to an oxidative environment (*Ox*) towards the core of the catalyst particle, and the outlet of a fixed bed reactor. If the FTS reaction active Fe_xC is oxidized to Fe_3O_4, pathway (5) may convert H_2O + CO to CO_2 + H_2 via the Water-gas Shift (WGS) reaction.

to the olefin formation. With increasing reaction temperature, the olefin content in total may not change or decrease,[1,27,91,93] or might even increase for K-promoted Fe-based catalysts.[27] Conversion of α-olefins into internal olefins increases with increasing reaction temperature.[27,91]

On Fe-based FTS catalysts, also the conversion of CO via the WGS reaction,[32,33,37] and via the Boudouard reaction increases with increasing reaction temperature.[1,42–44] This increases the total CO conversion, but away from the FTS reaction hydrocarbon products. The inactive carbon deposition from the Boudouard reaction increases roughly 50% for every 10 °C increase in the reactor bed temperature.[1] How the FTS reaction hydrocarbon production C pathways change in relative terms in comparison to the competing WGS and inactive carbon formation C pathways, against increasing temperature, is not clear for the time being.

3.2. Input H_2:CO Ratio

Increasing the FTS reaction input feed's H_2:CO ratio increases the hydrogenation ability of the catalyst material. This decreases the α-value via an increased probability for hydrocarbon chain termination and also, the olefin content decreases as any unsaturated C=C bonds are more likely to be hydrogenated.[1,27,91] Short-chained α-olefins are affected more than longer internal olefins, as the short α-olefins are more susceptible towards secondary hydrogenation reactions.[27,91] Also, an increasing input feed H_2:CO ratio, in general, decreases the inactive carbon deposition rate.[1,3,53] This, while keeping in mind the earlier mentioned exception of a small amount ($\approx$1%) of H_2 in the CO feed increasing the inactive carbon deposition in comparison to a pure CO input reactant.[1,43,50,51]

Despite the input feed H_2:CO ratio effect being rather clear – more input H_2 in relation to CO results in more hydrogenation activity – noteworthy emphasis is that the actual H_2:CO ratio over the different catalyst sites and bed positions may vary. Indeed, the conversion of H_2:CO in a ratio of ~2:1 (i.e., ideal FTS),[3,91] WGS activity in forward or reverse directions,[3,29,31,38–40,91] and the possibility of incorporating H and/or C to inactive carbon species,[42,43,47–49] can all modify the local ratio of H_2:CO along the catalyst particle as well as the reactor bed. The locally altered H_2:CO ratios can therefore affect the hydrocarbon selectivities during the FTS process.[1,3,56]

3.3. Gas Space Velocity

Increasing the reactor gas space velocity has the effect of increasing FTS reaction's hydrocarbon products' olefin content, especially in the short-chained α-olefins fraction. As the space velocity increases, the probability for olefin re-adsorption decreases, thereby decreasing secondary hydrogenation reactions.[1,27,91] The effects of catalyst particle size or catalyst extrudate size/shape on olefin re-adsorption are currently uncertain. The α-value remains unchanged with the changing space velocity.[1,91] The CO conversion decreases, while the FTS and WGS reaction rates, especially with Na and K promoted catalysts, increase with increasing space velocity.[34,35] As the FTS reaction hydrocarbon production rate increases faster than the WGS reaction rate,[34,35] relatively more CO is converted towards the desired hydrocarbon products at higher space velocities than is consumed by the WGS reaction.

3.4. Reaction Pressure

The effect of the total FTS reaction syngas H_2:CO pressure on the hydrocarbon product selectivity is more complex than the effects of the other FTS reaction process parameters. While for a Co-based FTS catalyst the CH_4 selectivity decreases with increasing H_2:CO pressure within the range of ~5–25 bar, no significant change in the CH_4 selectivity with changing reaction pressure is observed for a Fe-based FTS catalyst.[94] This holds when the reactor outlet H_2:CO ratio (i.e., ~ reactor H_2:CO ratio) is kept constant.[94] With increasing H_2:CO total pressure within the range ~15–25 bar, Todic et al. observed a somewhat increased α-value and decreased olefin content, but also the outlet H_2:CO ratio dropped, in this way affecting the hydrocarbon selectivities.[91] In experiments at Sasol with Fe-based FTS catalysts, both an increase in the α-value and an increase in the olefin content, as well as no change in either of the hydrocarbon selectivity variables with increasing H_2:CO reaction pressure, have been observed.[1]

An increase in the total H_2:CO pressure increases the activity of an Fe-based FTS catalyst.[94] This in turn can affect the actual reactor H_2:CO ratio as well as the partial pressures of H_2O and CO_2 via an increased CO conversion, thereby altering the hydrocarbon selectivities, as discussed above. In general, the effect of total reaction pressure on the Fe-based FTS hydrocarbon selectivities depend on the individual partial pressures of H_2, CO, H_2O and CO_2 present in the FTS reactor,[1,3,91,95] and their relation further depends on the used reaction temperature.[3,95]

With regard to the inactive carbon deposition, as briefly mentioned above, with the total reaction syngas pressure of $\gtrsim$ 15 bar with a H_2:CO ratio $\gtrsim$ 5, the inactive carbon formation can be suppressed.[1,53] This holds while improving the C pathway selectivity towards the FTS reaction hydrocarbon products.[1,53] With a lower input H_2:CO ratios of $\lesssim$ 1, the carbon deposition increases with increasing total reaction pressure.[53] According to Todic et al., the WGS reaction extent decreases with an increasing total FTS reaction pressure.[91]

4. Effect of Alkali-Sulphur Promotion

The addition of combined alkali-sulphur (alkali as Na or K) as chemical promoters for Fe-based FTS catalysts has the following effects: i) a decreased CH_4 selectivity to a lower value than predicted by the Anderson-Schulz-Flory (ASF) distribution when alkali and sulphur are present in an optimal ratio,[22,23] ii) a lesser increase in the hydrocarbon chain length (i.e., α-value) in comparison to if only alkali is added,[20,21,96] iii) an increased

hydrocarbon selectivity towards olefins,[20,22,23,97] and iv) an overall increased CO conversion.[23,82,96,98] Suppression of the CO_2 selectivity, without detrimentally affecting the hydrocarbon production, by addition of sufficient amount of sulphur to a K-containing Fe-based FTS catalyst has also been suggested.[99]

4.1. General H_2 and CO Adsorption Principles

The simplified effects of chemical promoters added as electropositive (e.g., Na or K) or electronegative (e.g., S) adsorbates on a transition metal (e.g., Fe) are (Figure 3):

i) Electropositive adsorbates donate electrons towards the transition metal surface, thereby decreasing the measurable surface work function; while the electronegative adsorbates do the opposite.[85,87,100]
ii) To modify the electrostatic potential near the transition metal surface, due to dipole moment formed between the – partly or fully ionized – chemical promoter adsorbate and the transition metal surface.[85,100]
iii) To possibly offer direct adsorption or reaction sites for reactants (e.g., H_2 or CO).[88,100–102]

Under FTS reaction relevant conditions on Fe_xC surface, both H_2 and CO adsorb dissociatively due to the electron back-donation from the (near-) zerovalent Fe d-orbitals to the antibonding C–O π^* and H–H σ^* molecular orbitals.[86–89,100–102] The dissociation of the adsorbed H_2 and CO on Fe_xC surface is affected by i) the availability of electrons in the Fe_xC d-orbitals for the back-donation and ii) the stability of the Fe_xC surface adsorbed, intermediate states of the H_2 and CO molecules.[86,89,100,101]

The addition of alkali elements in moderation increases the Fe d-orbital electron density and availability, i.e., it decreases the surface work function; while the addition of sulphur does the opposite.[86–89,100–102] Via the electrostatic interaction between the formed promoter-surface dipole moment and the reactant adsorbates, the electropositive alkali stabilizes the H_2^- and CO^- intermediate states on the Fe_xC surface, while the electronegative S destabilizes them.[86,89,100,101] Generally speaking, alkali as an individual chemical promoter in a Fe-based FTS catalyst increases the dissociative adsorption of H_2 and CO. While sulphur as promoter, individually, works vice versa decreasing the dissociative adsorption of H_2 and CO. The dissociative H_2 and CO adsorption promoting effects by K and the inhibiting effects by C, O and S over a surface of metallic state Fe have been experimentally observed by e.g. Benziger and Madix.[88]

Furthermore, with the added alkali to the Fe-based FTS catalyst, carbonate or formate species are commonly observed upon CO adsorption, species which are absent without alkali promotion.[100,103–107] Also, the direct interaction between the alkali and the metallic state Fe surface adsorbed H_2 and CO has been suspected, possibly aiding in the molecules' dissociation.[88,108,109] Similar alkali/CO interaction has also been noted for K promoted Al.[108]

Upon addition of alkali (as K), the desorption temperatures for adsorption products of H_2 and CO are increased at the expense of a lower temperature desorption.[88,101,102] That is, the added alkali increases the overall surface binding strength of H_2 and CO adsorption/desorption products. Within the FTS reaction relevant temperatures ($\lesssim 340\,^{\circ}C$), the H_2 adsorption products are more strongly bound than the CO products with the addition of alkali K.[88] The addition of electronegative adsorbates (e.g., S or O) has the opposite effect of lowering the desorption temperatures for the adsorbed products of CO and H_2.[88,101]

The measured adsorption energy change for an alkali K promoted Fe metal surface is higher for CO ($\approx +3.0$ kcal/mol) than for H_2 ($\approx +1.5$ kcal/mol).[102] Worth noting is that in an

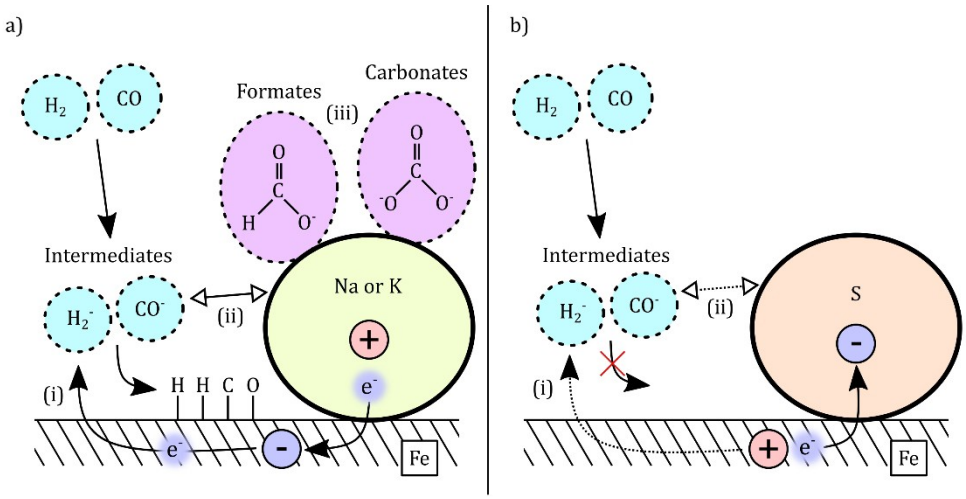

Figure 3. A schematic summary on the general effects of chemical promoter addition on H_2 and CO adsorption over the (near-)zerovalent Fe surfaces (e.g. α-Fe or Fe_xC). **With added electropositive alkali (as Na or K)**: a) (i) increased Fe surface electron density increases electron back-donation towards antibonding orbitals of Fe surface adsorbed intermediate H_2^- and CO^- states, (ii) formed alkali-Fe surface dipole moment stabilizes the intermediate H_2^- and CO^- states via electrostatic interaction, and also (iii) formation of formates and/or carbonates is observed. With alkali, both effects (i) and (ii) *increase* dissociative adsorption of H_2 and CO. **With added electronegative S**: b) (i) electron back-donation from Fe surface is weakened, and (ii) intermediate H_2^- and CO^- states are destabilized. With S, the effects (i) and (ii) *decrease* dissociative adsorption of H_2 and CO.

often cited study by Dry et al.,[110] the heat of H_2 chemisorption was found to decrease due to the addition of K promotion. That is, added K would inhibit H_2 adsorption, in contradiction to the present discussion. However, as noted by Benziger and Madix,[88] the results by Dry et al. were likely obtained on an oxide rather than on a Fe metal (or Fe carbide) surface and the observed H_2 inhibition effect was more likely due to the presence of O atoms rather than the presence of K atoms.[88]

Besides the arguments on the electropositivity and electronegativity of the added chemical promoter on H_2 and CO adsorption, also the alkali or sulphur adsorbate binding geometries on Fe surfaces can play a role.[88] Despite the fact that the O atom adsorbates are being more electronegative and the C atom adsorbates having a similar electronegativity as the S atom, the S atom adsorbates on metallic Fe surface showed a more pronounced inhibition effect on CO and H_2 adsorption than either O or C did. This effect was thought to be due to different binding geometries, which the O and C take versus the S adsorbates on the metallic Fe surface.[88] The different binding of O and S elements might be a very relevant factor when a combined Na–S promotion is applied in the FTS reaction.

4.2. Alkali in Fischer-Tropsch Synthesis

The most common chemical promoters added to a Fe-based FTS catalyst are K and Na.[1,19,34,81,96,111] Other alkali and alkaline earth elements have also been screened for the FTS reaction promotion, but K and Na remain the most suitable, in terms of both FTS reaction activity and selectivity.[34,36,81,95]

The addition of alkali by itself to a Fe-based catalyst has the effect on the FTS hydrocarbon selectivity of increasing i) the α-value and ii) the hydrocarbon product slate olefin content.[1,27,34,52,93,95,111] The alkali hydrocarbon selectivity effect is commonly attributed to an overall decrease in the catalyst's hydrogenation ability, i.e. it effect on the Fe_xC surface H:C ratio. The decreased H:C ratio results in a decrease in the hydrocarbon chain termination and in the olefin hydrogenation via primary or secondary pathways.[1,27,52,95,111]

The lowered H:C surface ratio with alkali addition can be explained as i) the adsorption energy is increased more for CO (+3.0 kJ/mol) than for H_2 (+1.5 kJ/mol).[102] Thus, CO is more preferably adsorbed than H_2 when H_2 and CO compete for the alkali-promoted Fe_xC surface adsorption sites. ii) the alkali promotor increases the elemental binding strength of H more than that of C on metallic Fe(/Fe_xC) surface.[88] The increased binding strength of H to the Fe_xC surface results in a depletion of the weakly bound H available for the FTS reaction.[112] Therefore, both alkali addition effects effectively decrease the Fe_xC H:C surface ratio available for hydrocarbon-forming FTS reactions.

Increasing the alkali promotion has the intrinsic tendency to increase the inactive carbon deposition C pathway via the Boudouard reaction, along the overall increased CO conversion and dissociation.[1,42,45] Although, a sufficiently low level of added alkali may nevertheless decrease the carbon deposition rate in comparison to an unpromoted Fe-based catalyst, this effect with still observable alkali promotion affects the FTS hydrocarbon selectivity.[1] Alkali also increases the WGS reaction rate,[52,111,113] consuming CO towards the WGS reaction products away from the FTS reaction.[34,36] Alkali furthermore promotes the WGS reaction even without the presence of a transition metal.[105,106] To sum up, as undesired effects from the alkali addition: C pathway selectivity towards FTS reaction hydrocarbon products decreases due to CO being consumed towards the WGS and/or inactive carbon depositing Boudouard reactions. Nevertheless, in the case of low input H_2:CO ratio, the WGS reaction may become the rate determining step for FTS as the hydrocarbon production becomes dependent on the H_2 from the WGS reaction.[34,35] In this case, the CO-consuming and alkali-promoted WGS reaction becomes a possibly useful property for a FTS catalyst material.[26]

4.3. Sulphur in Fischer-Tropsch Synthesis

The effect of sulphur in heterogeneous catalysis is a rather complex phenomenon.[87,90] Too much of added S compounds often result in a catalyst poisoning,[82,83,87,114] while small amounts of added S compounds may have beneficial FTS catalysis effects. S containing impurities in the CO gas can also gradually enrich on the catalyst, thus altering its behaviour.[45] From a review article by Madon and Shaw, some of the possible effects of the S addition on the FTS catalyst are:[87]

1) Avoiding reactor hotspots via decreased CO conversion;
2) Selective S adsorption on different reaction sites i.e. selectively affecting reaction pathways;
3) S itself may become an active site for reactions; and
4) S functions as an electron acceptor i.e. is an electronegative adsorbate on the transition metals and depletes the metals from electrons.

As mentioned earlier, the FTS reaction is an exothermic reaction and any hotspots created by the released heat to the reactor bed may cause the bed temperature to increase locally. This results in a decreased α-value, which most easily can be seen by an increased CH_4 selectivity, and/or the inactive carbon deposition via the Boudouard reaction. If a FTS reactor bed is operated non-isothermally, S poisoning decreases CO conversion eliminating the hotspots, which can result in an increased α-value (and therefore in a decreased production of CH_4) and in a decreased carbon deposition. That is, the listed point 1) is relatively easy to understand.

As examples of this effect, Dalla Betta, Piken and Shelef observed decreased catalyst activities with added S, as well as decreased CH_4 and increased C_{2+} selectivities and also discussed signs of possible non-isothermal reactor bed operation in their data.[115] Similar effects where S addition likely affects the initial reactor bed operating temperature, can be observed in the studies by van Dijk et al. and Zhou et al. with the Fe-based FTS reaction operated at 350 °C.[116,117] In the study by van Dijk et al., the added S prevented an initial spike of high FTS catalysis activity in comparison to the non-S containing catalyst. The added S likely prevented any excessive reactor bed

heating at the initiation of the FTS reaction, limiting the fast catalyst deactivation from excessive formation of inactive carbon species.[116] The same comments apply to the study by Zhou et al., who exposed their pre-reduced Fe-based FTS catalyst material to H_2:CO directly at 350 °C.[117] This is an initial reaction temperature too high for ensuring isothermal bed operation without excessive reactor bed heating.[71]

Definitely pinpointing the effect of the listed points 2), 3) and 4) and their possible combinations in relation to Fe-based FTS catalysis effects is a complex task. In addition, unfortunately, a variety of S poisoning studies with FTS reaction have been conducted with alkali-containing Fe-based catalysts. Thus, mixing both the FTS reaction promotion effects by alkali-S combination and possible poisoning by excessive S addition. This further complicates the task of discussing the S effects on the FTS reaction.

In several studies, positive S promotion effects in the Fe-based FTS reaction have been observed. However, in these studies, alkali-containing catalysts promoted, intentionally or inadvertently, with synthesis precursors or precipitation agents containing the alkali promoters, have commonly been used.[82,83,96,118–122] Washing of the prepared catalysts with deionized water in order to remove the alkali,[82,121] or possible S-ions,[121,123] is insufficient in order to have an alkali- or a S-free FTS catalyst material free of promotion or poisoning effects.

From a S poisoning study by Bromfield and Coville,[121] it can be pointed out that Na_2S was used as the S precursor and Na_2CO_3 as the catalyst precipitation agent. Despite the subsequent washing to remove the Na atoms from the precipitated Fe catalyst material, with low levels of added S, the catalytic FTS reaction results resemble of what would be expected for the Na–S promotion.[121] Presumably, the work led to a later Sasol patent on Na–S promotion with Fe-based FTS catalyst materials.[21]

Furthermore, in a study by Shultz et al., the initial S addition on K-containing catalysts resulted in an initial promotion effect by K–S, but this was followed by S poisoning effects when too much of S was added.[83] In the study, with a low level of COS added as the S-bearing gas compound, a slight increase in the hydrocarbon products olefinicity could be observed. Despite the increased reaction temperature, there was no increase in the CH_4 selectivity. Both effects can be explained by K–S promotion. Further addition of COS increased the CH_4 selectivity (and seemingly decreased the α-value), this despite the simultaneously decreased reaction temperature, which should decrease the CH_4 selectivity. And also simultaneously with the increasing amount of S addition, the olefin selectivity decreased for the catalyst.[83] The S poisoning effects of decreased olefin content and increased CH_4 formation can also be observed when different experimental runs with the same reaction temperature are compared.[83] Similar observations have been made by Botes et al., i.e., excessive S addition on alkali containing Fe-based catalysts increases the CH_4 selectivity in the FTS reaction.[22]

In the simplest way expressed, the "promotion effects" of increasing CH_4 selectivity and decreasing olefin content by S poisoning of alkali-containing catalyst material can be explained as S being an electronegative adsorbate. That is, the functioning in an opposite way to the alkali addition (Figure 3).[87] The S addition thus likely increases the overall H:C surface ratio resulting in an increased hydrocarbon hydrogenation and chain termination reactions. However, it is unclear how the S effects, which are not directly related to the S elements electronegativity, i.e. the points 2) and 3) mentioned above, affect the observed selectivities in the Fe-based FTS reaction. Generally speaking, the adsorbate S might selectively block some geometric reaction sites, such as active steps. This might affect the reaction rates and pathways to different degrees in the FTS reaction.[87,90] Some evidence has been observed on the effect of site-blocking for some model catalytic systems.[90] However, how the data obtained from ultra-high vacuum model experiments compares to a more dynamic Fe-based FTS catalyst material behaviour at higher reaction pressures, is still uncertain.[90]

As an excessive addition of S eventually covers the active Fe_xC surface decreasing its FTS reaction activity,[83,118,119,121,122] and CO dissociation capability,[45,124] it is unlikely that S itself performs as an active site for the FTS reaction. However, some cautious doubt can be expressed as observations of the S compounds possibly assisting in dehydrogenation reactions with Fe-based catalyst materials have been made.[125]

In contrast to the cited *alkali-containing* Fe-based catalyst material studies on the S effects in the FTS reaction, when catalyst precursors *free of alkali* have been used, the catalyst is directly poisoned by a low level of S addition. S poisoning effects of decreasing: i) α-value,[84] ii) olefin content versus paraffins,[84,116] and iii) overall CO conversion,[82,84] have been observed. Interestingly in the study by Xu et al. with an alkali-free Fe-based catalyst, the CH_4 selectivity remained virtually unaffected despite the increasing S content and decreasing α-value.[84] This seems to be in contrast to the Fe-based, alkali-containing catalyst materials for which the CH_4 selectivity increases with excessive addition of S.[22,83]

In terms of the various C pathways operative, the effect of the added S might be simply to decrease the overall CO and H_2 dissociation, without altering the relation between the C pathway selectivities. Although the overall carbon deposition decreases with added S,[45,124,126,127] so does the CO conversion.[84] That is, whether S truly suppresses carbon deposition without decreasing the FTS reaction hydrocarbon production, as is sometimes discussed, needs to be compared in relative terms to the CO converted to FTS reaction hydrocarbon products. Such studies do not seem to exist at the moment in the open literature.

On Fe-based WGS reaction catalysts, S behaves as a poison.[33,37] Thus, unlike alkali, S does not promote the WGS reaction.

4.4. Alkali-Sulphur in Fischer-Tropsch Synthesis

In light of individual alkali and sulphur promotion properties with respect to the FTS reaction hydrocarbon selectivities: *the combined alkali-S promotion effect resembles both.* The increased

olefin selectivity and CO conversion are "alkali-like", while the decreased α-value in comparison to alkali-only addition is "sulphur-like". The unique effect of decreased CH_4 selectivity to a lower value than expected from the ASF-distribution is solely a combined alkali-sulphur effect.[22] Together these effects enable an increased yield towards short-chained C_2-C_4 olefins.[20–23]

The unique disruption of the lowered CH_4 selectivity has been proposed to be due to a changing binding geometry of the chemical promoter compound when the S is added as a counter-ion for the alkali promoter.[24] Commonly, the alkali is thought to be in an oxidized form under the FTS reaction conditions, although the exact chemical compound is uncertain.[100,110] Benziger and Madix have observed the oxidation of K atoms by O from CO dissociation in their science studies on metallic Fe surface, in support of the thought for K oxidation.[88]

The added S to Na promotion likely replaces the O as the alkali's counter-ion resulting in a Na–S compound instead of a Na–O phase.[24] From a combination of experimental data and theoretical calculations, thereby applying Density Functional Theory (DFT), Xie et al. concluded that the counter-ion change from O to S i) increases the Na electron donation towards Fe atoms as S is less electronegative than O; and ii) changes the Na–S promoter compound binding geometry on the Fe_xC surface. The combined effect decreases the availability of H for the hydrogenation reactions, resulting in especially a suppressed formation of CH_4.[24]

As mentioned before, Benziger and Madix have discussed the individual difference between O (and C) and S adsorbates on a metallic Fe surface.[88] Their experimental results and discussion are in support of the different binding modes for O and S. The S adsorbates bind on the metallic Fe surface in a manner, which more effectively inhibits the adsorptive dissociation of H_2 and CO than do O adsorbates, despite O being more electronegative and Fe surface electron depleting than S.[88] The experimental surface science results from Benziger and Madix thus make similar suggestions as do the theoretical results by Xie et al..

Combined alkali-sulphur promotion affects the C reaction pathways for the dissociated CO by: increasing the overall CO conversion,[23,82,96,98] and might also increase, at least the initial, carbon deposition rate.[96,98,127] Although, in the cited studies regarding the carbon deposition, the vast differences in the CO conversion levels have not been accounted for between the different catalysts and promotion levels. The source for inactive carbon deposited on the catalysts is CO. For low CO conversion carbon deposition is necessarily low and vice versa. For meaningful comparison of carbon deposition between various alkali-S promoted catalysts: the carbon deposition needs to be normalized to the total (i.e. integral of) CO conversion over the measurement period. Otherwise, the carbon deposition results can be misleading and the conclusions misguided.

Nevertheless, as significant CO_2 selectivity in the FTS reaction has been observed in the presence of alkali-sulphur promotion with Fe-based catalysts:[23,96,98,127] either increased WGS and/or carbon-depositing Boudouard reactions, both releasing CO_2, can be suspected to be operative. An increased CO_2 selectivity with the presence of alkali-sulphur promotion would be akin to the earlier discussed alkali-only addition of increasing WGS and carbon deposition reactions, therefore, being an "alkali-like" property. Moreover, after experiments at Sasol, Botes et al. suggest that the CO conversion selectivity towards FTS reaction hydrocarbon production decreases with the added alkali-sulphur promotion. However, precise data on this observation were not given.[22]

In precisely quantified terms, how the alkali-sulphur promotion affects the WGS reaction or the inactive carbon depositing Boudouard reaction, in relation to the FTS reaction hydrocarbon production, remains unclear for the time being.

Summarizing the aspect of promotion, Figure 4 gives a schematic overview on the effects of alkali (Na or K), S and combined alkali-S and their effect on the FTS hydrocarbon and C pathway selectivities, while Table 2 further summarizes the

Table 2. The effects of various Fischer-Tropsch Synthesis (FTS) reaction process parameters and alkali, sulphur and alkali-sulphur chemical promoters on the C reaction pathways and on the FTS hydrocarbon selectivity in the Fe-based FTS reaction.

Parameter	Hydrocarbon Selectivity			CO	C Pathway Selectivity		
	CH_4	α-value	Olefins	Conversion	FTS	WGS	Carbon Deposition
Temperature	↑	↓	∽	↑	∽	↑	↑
H_2:CO	↑	↓	↓	∽	∽	∽	↓
Space Velocity	∽	↔	↑	↓	↑[a]	↓	∽
Total Pressure	∽	∽	∽	↑	∽	↓	↑[b]
Alkali	↓	↑	↑	↑	↓	↑	↑[c]
Sulphur	∽[d]	↓	↓	↓	∽	∽	∽[e]
Alkali-Sulphur (~2:1)	↓[f]	↑[g]	↑	↑	∽	∽[h]	↑[h,i]
Symbols:	↑ or ↓ – increasing or decreasing FTS reaction property against increasing parameter.						
	↔ – no effect.						
	∽ – complex or unclear effect.						
Alkali:	Na or K atoms as added promoters.						

[a] The FTS reaction rate increases faster than the Water-gas Shift (WGS) reaction rate with increasing space velocity. [b] With $\gtrsim$ 15 bar total reaction pressure and 5 $\gtrsim$ H2:CO ratio carbon deposition can be suppressed. [c] The low addition levels of alkali may not increase the carbon deposition rate and might even lower it. [d] Excessive sulphur addition increases the CH4 selectivity, if alkali is present. [e] Commonly, a decrease is observed, likely, due to the overall decrease in CO conversion. [f] The selectivity towards CH4 can be suppressed to a value below the Anderson-Schulz-Flory (ASF) distribution expectations. [g] The α-value is increased less than with only alkali addition. [h] The selectivity towards CO_2 with alkali-sulphur promotion increases. [i] At least, the initial carbon deposition rate at the start of the FTS reaction might increase.

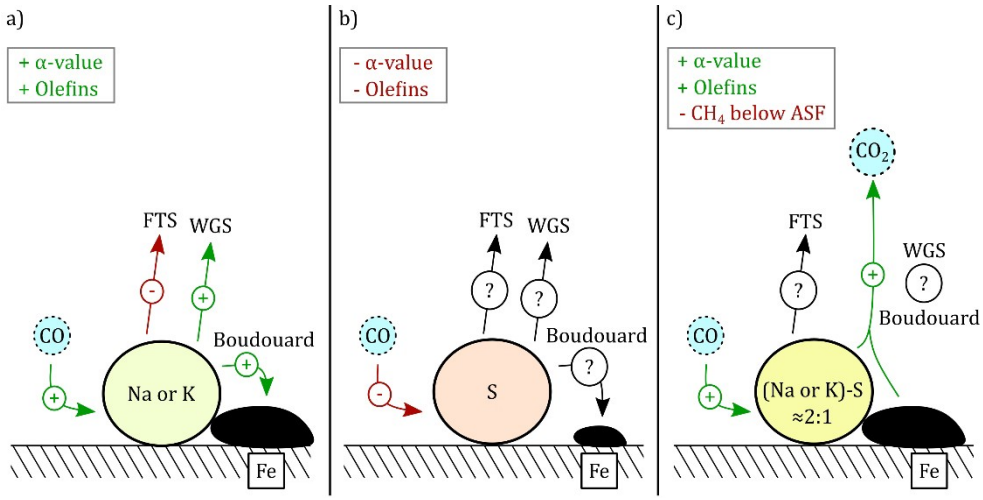

Figure 4. A schematic summary on the effects of chemical promoters on (near-)zerovalent Fe surfaces (e.g. α-Fe or Fe_xC). The effects of a) alkali (as Na or K), b) S and c) alkali-S in molar ratio of 2:1 in Fe-based Fischer-Tropsch Synthesis (FTS) reaction, on FTS hydrocarbon product and C pathway selectivities and on overall CO conversion. Green – increased, Red – decreased, and ? – an unknown change in the property in comparison to an unpromoted catalyst material. The combined c) alkali-S promotion increases CO_2 selectivity, likely indicating increased Water-gas Shift (WGS) and/or Boudouard reaction C pathway selectivities.

effects of all of the discussed FTS reaction process parameters together with the effects of the alkali, S and alkali-S chemical promoters in the Fe-based FTS reaction.

5. Fe Carbides in Fischer-Tropsch Synthesis

The most common Fe carbide observed in the FTS reaction related research is the χ-Fe_5C_2 phase, which is also known as the Hägg carbide. The so-called "ε-carbides" (or (pseudo-) hexagonal) Fe carbides are also often observed and labelled as ε′-$Fe_{2.2}C$, Fe_2C, ε-Fe_2C or ε-Fe_3C in the literature. Less common Fe carbides encountered under FTS reaction conditions are θ-Fe_3C (cementite) and Fe_7C_3 (the Eckström-Adcock carbide). The mentioned Fe carbides, while excluding the Fe_7C_3 phase, are also commonly formed as unwanted precipitates during tempering (i.e. heat-treating) of martensitic steels. Fe carbide unit cells in this section are visualized with the VESTA software.[128]

5.1. "ε-carbides" (ε-Fe_3C and η-Fe_2C)

The so-called "ε-carbides" or Fe carbides with (pseudo-) hexagonal Fe lattices have traditionally been the most difficult Fe carbides to identify due to an unfortunate confusion with the labelling and identification of the ε′-$Fe_{2.2}C$, (ε-)Fe_2C and ε-Fe_3C phases. It is often unclear to which actual crystal lattice/structure the used nomenclature, as per author, refers to.

The ε-Fe_3C phase has been identified by Nagakura.[68] In their Electron Diffraction (ED) study on Fe thin-films, the author solved the diffracting Fe carbide structure to have a space group of hexagonal *P6₃22* (182). This Fe lattice is hexagonally ordered and the C atoms occupy a one third of the octahedral interstitial Fe spaces in a disordered manner (Figure 5). The disordered C packing was observed from the broadening of the superstructural diffraction peaks, which for the Fe carbides originate from the interstitial C atoms. By decomposing the formed ε-Fe_3C phase to α-Fe and graphite by heating it under vacuum, its stoichiometry was estimated to be around $Fe_{2.8}C$.[68]

As commented by Nagakura,[68] the studied ε-Fe_3C phase had the same lattice parameters, when ignoring the weak superstructural C diffraction, as a Fe carbide labelled as "Fe_2C" with hexagonal Fe lattice observed earlier by Hofer, Cohn and Peebles.[61] That is, the earlier "hexagonal Fe_2C" and Nagakura's ε-Fe_3C were the exact same carbide.

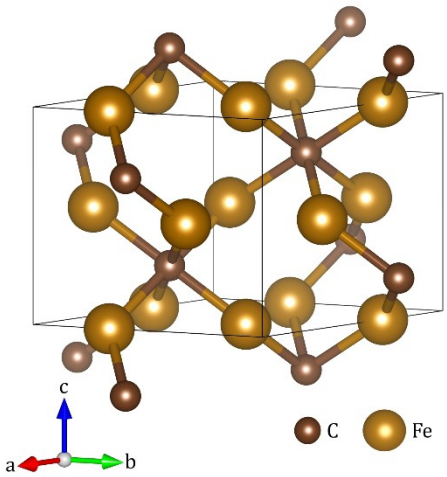

Figure 5. The unit cell of the hexagonal ε-Fe_3C *P6₃22* (182). The Fe lattice is purely hexagonal and the C atoms occupy third of the octahedral Fe lattice interstitial spaces in a random, distorted manner.

The stoichiometry for Hofer's Fe_2C was determined by a comparison to – what at the time was thought to be – isomorphism with a "Hägg carbide Fe_2C". Experimental C:Fe ratio for the carbide was further determined by the *total sample weight* increase upon carburization.[61] Both, in retrospective, are inaccurate assumptions for determining a carbide's stoichiometry. Later on, after more accurate structural solutions were provided for the Hägg carbide,[129] the original assumptions in the identification of the "hexagonal Fe_2C" and its stoichiometry were acknowledged by the researchers at the time to be inaccurate.[130] No evidence of an Fe carbide as "hexagonal Fe_2C" exists as after Hofer, Cohn and Peebles.[61] Unfortunately, the acknowledgement of the mistaken original labelling went unnoticed and several later studies cite a "hexagonal Fe_2C" carbide originating from the study by Hofer, Cohn and Peebles.[66,131,132] This has resulted in some unfortunate confusion in the characterization of the actual Fe carbide phases in the FTS reaction.

Furthermore, unfortunately, in a French written study by Dirand and Afqir,[133] the "Fe_2C" carbide with the data from the study of Hofer, Cohn and Peebles was solved to have a space group of hexagonal *P6₃/mmc* (194). Dirand and Afqir also acknowledged the existence of the ε-Fe_3C phase indexed as *P6₃22* (182) after Nagakura, but unfortunately did not acknowledge that the carbides were the same.

The reason why the same carbide was solvable with different space groups is due to the originally used diffraction techniques to collect the data. The ED pattern by Nagakura contains *the diffraction originating from both Fe and C* in the crystal lattice. The X-ray Powder Diffractometry (XRPD) data collected by Hofer, Cohn and Peebles is not sensitive to the low atomic number element C and essentially, only *the diffraction from Fe* was observable. Thus, the *P6₃22* (182) is the full, proper space group with Fe and C diffraction while the *P6₃/mmc* (194) is an incomplete space group only for the Fe diffraction, for the same hexagonal ε-Fe_3C phase observed by both Nagakura and Hofer, Cohn and Peebles.[61,68]

The International Centre for Diffraction Data Powder Diffraction File-4+ (ICDD-PDF-4+) database lists the Dirand and Afqir's solution based on Hofer, Cohn and Peebles's unit cell as a Fe carbide with space group *P6₃/mmc* (194) with database number 00-036-1249. As discussed above, Nagakura's crystal structure solution with space group *P6₃22* (182) and database number 04-008-9572 should be used instead. Dirand and Afqir's *P6₃/mmc* (194) incomplete lattice solution should not be used in order to avoid any unnecessary confusion for the future identification of the ε-Fe_3C phase.

Nagakura's ε-Fe_3C is not the only Fe carbide phase observed with a (pseudo-)hexagonal Fe lattice. In a spent FTS catalyst material, Barton and Gale observed a similar hexagonal Fe carbide to what Hofer, Cohn and Peebles observed earlier. However, the Fe carbide differed from the previous observations by i) having split XRPD peaks, suggesting that a distortion from the hexagonal Fe lattice was present, and by ii) having significantly different unit cell parameters.[134] As XRPD was used, Barton and Gale could not conclusively solve the observed Fe carbide structure or the space group due to the missing superstructural diffraction from the interstitial C atoms. Barton and Gale assumed a stoichiometry of Fe_2C after the study by Hofer, Cohn and Peebles for their carbide.

Barton and Gale, however, calculated from their XRPD data that instead of having a purely hexagonal Fe lattice with lattice parameter $\gamma = 120°$, their observed Fe carbide crystal lattice had a distortion from the Fe lattice hexagonality where $\gamma = 120.92°$. This angle distortion accounting for the observed peak splitting in the X-ray diffraction patterns. As possible space group solutions for the crystal lattice, Barton and Gale gave trigonal $P\bar{3}m1$ (164), hexagonal *P6₃/mmc* (194) and orthorhombic *Pbcn* (60).[134]

From tempering studies on martensitic steel, Hirotsu and Nagakura solved a Fe carbide crystal structure on the basis of its electron diffraction patterns,[135] which resembled the earlier hexagonal ε-carbide (i.e., the ε-Fe_3C phase) observed by Hofer, Cohn and Peebles and Nagakura.[61,68] However, the Fe carbide was different to Hofer, Cohn and Peeble's observations as the Fe lattice was not purely hexagonal but rather a pseudo-hexagonal one with the Fe lattice distorted from hexagonality. Hirotsu and Nagakura labelled their Fe carbide as η-Fe_2C with an orthorhombic space group *Pnnm* (58) (Figure 6).[135] The C atoms in η-Fe_2C structure occupy half of the octahedral interstitial spaces in the Fe lattice, in a regular manner.[135] Hirotsu and Nagakura have proposed orthorhombic unit cell dimensions, after their η-Fe_2C phase, for the Fe carbide observed by Barton and Gale.[136]

The crystal structures of the ε-Fe_3C and η-Fe_2C phases, with the unit cell by Hirotsu and Nagakura corresponding to the Barton and Gale's Fe carbide, are depicted in Figure 7. The carbides indeed have very similar hexagonal Fe planes with differences of, that for i) η-Fe_2C $\gamma = 120.47°$ instead of $\gamma = 120.0°$ as for the purely hexagonal lattice of ε-Fe_3C and ii) there are no empty octahedral interstitial Fe lattice spaces in the lattice of η-

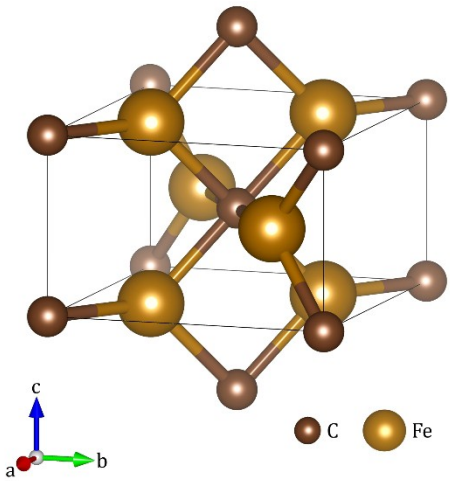

Figure 6. The unit cell of the orthorhombic η-Fe_2C *Pnnm* (58). The Fe lattice is distorted from hexagonality and the C atoms occupy half of the octahedral Fe lattice interstitial spaces in an ordered manner.

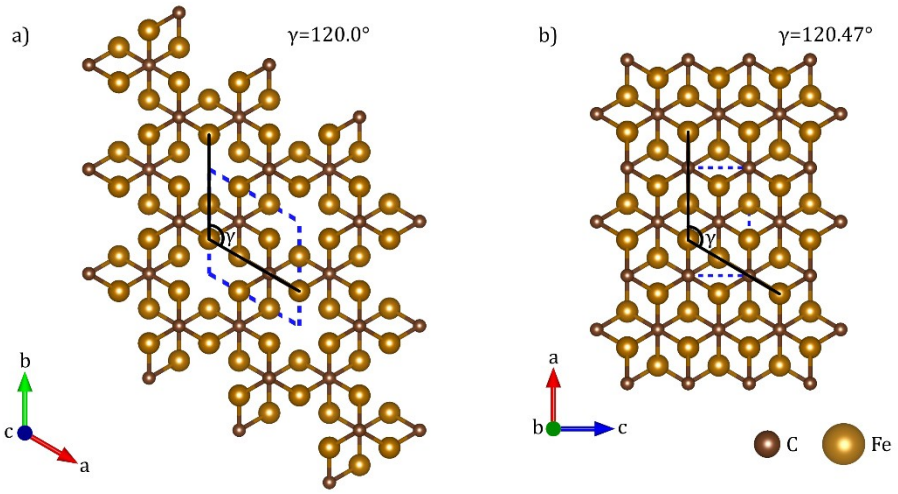

Figure 7. The crystal lattices of a) the hexagonal ε-Fe_3C *P6₃22* (182) viewed along the c-axis, b) the orthorhombic η-Fe_2C *Pnnm* (58) viewed along the b-axis, so that the (distorted-)hexagonal Fe planes are in plane with the paper. The η-Fe_2C unit cell is after Hirotsu and Nagakura corresponding the Fe carbide by Barton and Gale.[136] ***Blue, dashed line*** – the respective unit cells for each crystal lattice, ***Black, solid line*** – In plane Fe atom positions used for measuring the lattice angle parameter γ. For the ε-Fe_3C $\gamma = 120.0°$ i.e. the Fe lattice is hexagonal, while for η-Fe_2C $\gamma = 120.47°$ i.e. the Fe lattice is distorted from hexagonality. In the η-Fe_2C lattice the interstitial Fe spaces are occupied by C to a higher degree than in the ε-Fe_3C lattice.

Fe_2C. The crystal structures of ε-Fe_3C and η-Fe_2C are similar and closely related.

That is, the orthorhombic structure of the η-Fe_2C phase with the orthorhombic unit cell dimensions proposed by Hirotsu and Nakagura is a proper solution for the Fe carbide observed by Barton and Gale. It is the crystal structure for what is occasionally labelled in the literature as a pseudo-hexagonal (ε′-$Fe_{2.2}C$ or Fe_2C) Fe carbide phase.[59,137] The crystal structure for the η-Fe_2C phase by Hirotsu and Nakagura is listed with database number 04-013-9510 in the ICDD-PDF-4+2016 database.

To summarize the discussion so far, the labelling of a Fe carbide in the FTS reaction as (ε-)Fe_2C phase is improper and should not be used further as there is no evidence that such a Fe carbide exists. What can be grouped as the "ε-carbides" are two different carbides: ε-Fe_3C with hexagonal space group *P6₃22* (182) in which the Fe lattice is purely hexagonal and C atoms occupy a third of the octahedral Fe interstitial spaces in a random, disordered manner; η-Fe_2C with orthorhombic space group *Pnnm* (58) where the Fe lattice is distorted from the hexagonal symmetry and C atoms occupy half of the octahedral Fe interstitial spaces in a regular, ordered manner. A "pseudo-hexagonal Fe carbide" either labelled as a Fe_2C or ε′-$Fe_{2.2}C$, should not be used to describe a Fe carbide with distorted Fe lattice but rather the orthorhombic η-Fe_2C should be used instead. The crystal lattice of the η-Fe_2C phase contains the distorted (pseudo-)hexagonal Fe lattice.

5.2. Hägg Carbide (χ-Fe_5C_2)

The most commonly observed Fe carbide in the FTS reaction is the χ-Fe_5C_2 phase, which is mostly properly and consistently identified. The first observations of the Hägg carbide dates back to 1934,[138] and the carbide's crystal structure was later solved to be monoclinic, with a stoichiometry of Fe_5C_2.[129] Retief has further improved the accuracy of the structural solution for the known χ-Fe_5C_2 phase with a monoclinic space group *C2/c* (15) (Figure 8).[139] Du Plessis et al. have argued that the proper space group for the χ-Fe_5C_2 phase is not a monoclinic *C2/c* (15) but a triclinic $P\bar{1}$ (2).[140] However, Leineweber et al. have explained the observations by du Plessis et al. being due to anisotropic microstrain broadening rather than a different unit cell symmetry.[141] The crystal structure solved by Retief is a proper solution for the Hägg carbide χ-Fe_5C_2 and is listed in the ICDD-PDF-4+2016 database with number 00-051-0997. The crystal structure solutions provided by Leineweber et al. are also accurate for the Hägg carbide.[141]

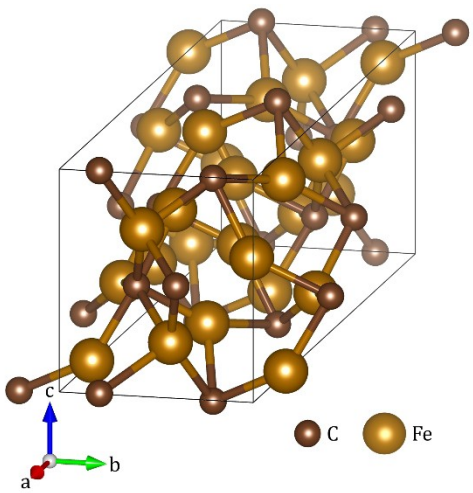

Figure 8. The unit cell of the monoclinic χ-Fe_5C_2 *C2/c* (15) (the Hägg carbide).

5.3. Cementite (θ-Fe_3C)

As being the most thermally stable Fe carbide,[57,142] cementite θ-Fe_3C is – akin to χ-Fe_5C_2 – a well-studied and consistently identified Fe carbide phase. Already the early studies have identified the cementite θ-Fe_3C crystal structure with an orthorhombic space group *Pnma* (62).[143] Later, Wood et al. have applied Neutron Powder Diffraction (NPD) to further improve the cementite θ-Fe_3C structure solution. These experiments provide to date the most accurate crystal structural solutions for the θ-Fe_3C phase, at various temperatures.[69] The crystal structure of θ-Fe_3C by Wood et al., at room temperature, is available in the Crystallography Open Database (COD) with the database number 9014027 (Figure 9).[144]

5.4. Eckström-Adcock Carbide (θ-Fe_7C_3)

The Eckström-Adcock carbide is rather rarely observed in the FTS reaction, but has been known to exist since the initial observations of a new carbide by Eckström and Adcock.[145] It may form during the FTS reaction after extended times under industrial high-pressure reaction conditions.[1]

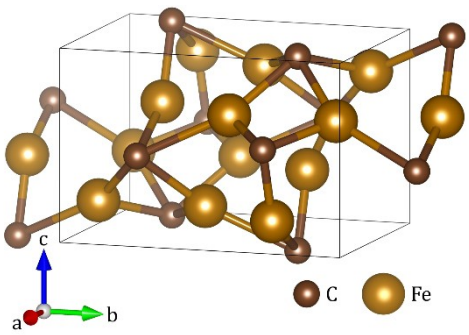

Figure 9. The unit cell of the orthorhombic θ-Fe_3C *Pnma* (62) (cementite).

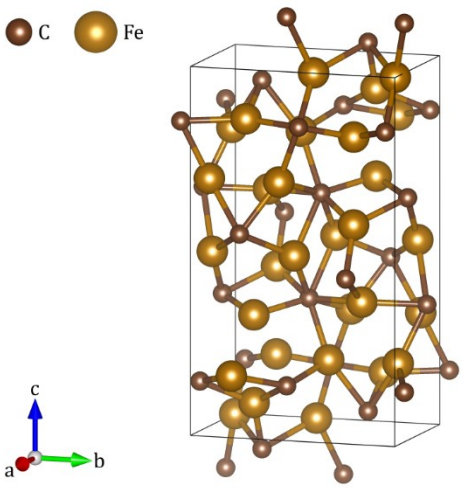

Figure 10. The unit cell of the orthorhombic θ-Fe_7C_3 *Pnma* (62) (the Eckström-Adcock carbide).

The initial identification of the carbide observed by Eckström and Adcock was done as a hexagonal Fe_7C_3 with a space group *P6₃mc* (186) by Herbstein and Snyman.[146] However, in later studies Fruchart et al. proposed the crystal structure of Fe_7C_3 to be an orthorhombic *Pnma* (62).[147] In a single crystal ED study by Audier, Bowen and Jones, the orthorhombic space group was agreed over the hexagonal one.[148] Therefore, the preferred crystal structure for the Eckström-Adcock carbide Fe_7C_3 has an orthorhombic space group *Pnma* (62) by Fruchart et al. (Figure 10).[147] The orthorhombic crystal structure for the Fe_7C_3 phase is available in the ICDD-PDF-4+ database with the database number 04-002-8165.

To make the distinction and to avoid any confusion between the Fe_7C_3 crystal lattices, the orthorhombic Fe_7C_3 *Pnma* (62) is arbitrarily labelled as θ-Fe_7C_3 akin to same space group θ-Fe_3C. The use of various Greek prefix letters,[149] to name the Fe carbides is rather arbitrary and not systematic.

The crystal lattice details for the discussed Fe carbides observable in the FTS reaction research i.e. ε-Fe_3C, η-Fe_2C, χ-Fe_5C_2, θ-Fe_3C and θ-Fe_7C_3 are listed in the Table 3. The crystal structure solutions are available from the listed authors in Table 3 and either the ICDD-PDF-4+ or COD databases.

5.5. Fe Carbide Hyperfine Fields

Just as was the case with their X-ray and electron diffraction data based crystal lattice solutions, the literature data with various Fe carbides identified in FTS research with Mössbauer Absorption Spectroscopy (MAS) can be challenging to follow due to the unclear nomenclature, as per author.

As based on the solved crystal structures for the Fe carbides, by the authors listed in Table 3, the total count and the site ratios for the crystallographically non-equivalent Fe positions can be determined. Each non-equivalent Fe position should ideally give a distinct MAS hyperfine field component with fields' spectral contribution ratios following the non-equivalent Fe site ratios.[150] Determining the non-equivalent Fe positions from the crystal structures gives the ideal Fe site ratios as: i) the ε-Fe_3C and η-Fe_2C phases have one equivalent Fe position, ii) the χ-Fe_5C_2 phase has three non-equivalent Fe positions in ratio of 2:2:1, iii) the θ-Fe_3C phase has two non-equivalent Fe positions in ratio 2:1 and iv) the θ-Fe_7C_3 phase has five non-equivalent Fe positions in ratio 2:2:1:1:1.

Le Caër et al. have discussed the MAS hyperfine field assignment of the "ε-carbides" on the basis of experimental data gathered from literature.[60] As Le Caër et al. note, the "ε-carbides" can be grouped around two hyperfine field values of 24.5±0.8 T and 17.2±0.3 T (at room temperature). Furthermore, increasing the amount of interstitial C atoms in the Fe lattice decreases the measured hyperfine field.[60,151–153] Thus, the field 24.5±0.8 T belongs to a "ε-carbide" with a low C content and the field 17.2±0.3 T for a "ε-carbide" with a higher C content. Recalling from the earlier discussion on the crystal

Table 3. The crystal lattice details of the Fe carbides encountered in Fe-based Fischer-Tropsch Synthesis (FTS) reaction with author references for the most accurate crystal structure solutions up-to-date. All lattice parameters are at room temperature. It is advised that the nomenclature of ε'-$Fe_{2.2}C$ or (ε-)Fe_2C should not be used for describing any of the Fe carbides.

Fe Carbide Phase	Space Group	Lattice Parameters [Å]	[°]	Database Number ICDD-PDF-4+ (2016)	Author
ε-Fe_3C	Hexagonal, $P6_322$ (182)	a = 4.767 b = 4.767 c = 4.354	α = 90 β = 90 γ = 120	04-008-9572	Nagakura (1959) [68]
η-Fe_2C	Orthorhombic, Pnnm (58)	a = 4.704 b = 4.318 c = 2.830	α = 90 β = 90 γ = 90	04-013-9510	Hirotsu (1972) [135]
η-Fe_2C[a]	Orthorhombic, Pnnm (58)	a = 4.862 b = 4.360 c = 2.755	α = 90 β = 90 γ = 90	-	Hirotsu (1974) [136]
χ-Fe_5C_2	Monoclinic, C2/c (15)	a = 11.588 b = 4.579 c = 5.059	α = 90 β = 97.746 γ = 90	00-051-0997	Retief (1999) [139]
θ-Fe_3C	Orthorhombic, Pnma (62)	a = 5.081 b = 6.754 c = 4.515	α = 90 β = 90 γ = 90	9014027[b]	Wood (2004) [69]
θ-Fe_7C_3	Orthorhombic, Pnma (62)	a = 4.540 b = 6.879 c = 11.942	α = 90 β = 90 γ = 90	04-002-8165	Fruchart (1965)[c] [147]

[a] Lattice parameters are translated according to Hirotsu and Nagakura,[136] to correspond the distorted Fe carbide observed by Barton and Gale.[134] [b] Crystallography Open Database (COD) number. [c] The original article written in French by Fruchart et al. is not readily available but some discussion on the crystal structure can be found in publication by Audier, Bowen and Jones.[148]

structures of the Fe carbides: for the ε-Fe_3C phase third of the interstitial Fe lattice sites are occupied by C atoms, while for the η-Fe_2C phase half of the interstitial sites are occupied by C. That is, the η-Fe_2C phase has the higher C content in its crystal structure. Therefore, the hyperfine field 24.5 ± 0.8 T is assigned for the one equivalent Fe site in the ε-Fe_3C crystal structure and 17.2 ± 0.3 T for the one Fe site in the η-Fe_2C phase. Occasionally, also an additional minor intensity hyperfine field at ~13.0 T has been assigned for "ε-carbides".[60,154,155] However, whether this is correct and from where the low ~13.0 T hyperfine field arises from, is uncertain. The two assigned hyperfine fields are the primary ones for the ε-Fe_3C and η-Fe_2C phases for correctly identifying the carbides.

The experimentally assigned, averaged hyperfine fields from the cited studies, for the Hägg carbide χ-Fe_5C_2 are the fields 21.4 ± 0.3 T, 18.1 ± 0.4 T and 10.9 ± 0.9 T with respective spectral contribution ratio of ~2:2:1.[59,77,155,156] The spectral contribution ratio is in agreement with the expected non-equivalent Fe site ratios for the χ-Fe_5C_2 phase. In addition to the commonly assigned hyperfine fields, Barinov, Protasov and Surikov have proposed an additional field of ~16.0 T to account for a possible anisotropy in the χ-Fe_5C_2 crystal structure.[156] The proposal by Barinov, Protasov and Surikov perhaps could account for the earlier discussed anisotropy phenomena, as observed by Leineweber et al. for the χ-Fe_5C_2 phase.[141] However, whether or not such anisotropy is present, the three assigned hyperfine fields are sufficient for identifying the χ-Fe_5C_2 phase.

The experimentally assigned, averaged hyperfine fields for cementite θ-Fe_3C can be obtained from studies by Bi et al. and Kniep et al. and have values of 20.8 ± 0.3 T and 20.0 ± 0.3 T.[157,158] However, as the values are very close to each other, commonly only one average hyperfine field value of 20.8 ± 0.5 T is used for the MAS fitting of θ-Fe_3C.[59,132,159,160] Neither Bi et al. nor Kniep et al. report the MAS-based relative spectral contribution areas for the θ-Fe_3C assigned hyperfine fields. Thus, how the crystallographically expected 2:1 non-equivalent Fe site ratio is assigned to the hyperfine fields, is unclear for the time being for the θ-Fe_3C phase.

The assignment of the hyperfine fields from the experimental literature data for the θ-Fe_7C_3 phase is problematic as the carbide is less often observed than the other carbides, and therefore less studied. For the orthorhombic crystal lattice of the θ-Fe_7C_3 phase, five non-equivalent Fe sites are expected with corresponding hyperfine fields. However, only three fields have been experimentally assigned so far in the literature. Averaging the hyperfine fields from the studies of Bi et al. and Yamada et al. gives field assignments as 22.9 ± 0.1 T, 18.5 ± 0.1 T and 16.3 ± 0.1 T.[157,160] Bi et al. have also assigned a fourth field for their (θ-)Fe_7C_3 phase as 21.0 T which might belong to the θ-Fe_3C impurity from the sample synthesis.[157]

In a theoretical MAS study, Liu et al. have predicted the hyperfine fields of 22.9 T, 22.9 T, 19.9 T, 18.7 T and 17.4 T for the orthorhombic θ-Fe_7C_3 phase.[153] The assignments by Liu et al. are relatively close to the experimental assignments by Bi et al..[157] That is, if the hyperfine field 21.0 T is assumed belonging to the θ-Fe_7C_3 phase rather than an impurity θ-Fe_3C phase and if the same field of 22.9 T is indeed assignable for two non-equivalent Fe positions. Bi et al. considered the Fe_7C_3 phase to only have three non-equivalent Fe sites,[157] as based on the hexagonal Fe_7C_3 structure by Herbstein and Snyman.[146] However, as discussed earlier, the hexagonal crystal lattice for the Fe_7C_3 phase is not a fully satisfactory crystal structure solution as based on the diffraction studies. The orthorhombic θ-Fe_7C_3 crystal structure should be used instead.[148] None of the cited studies assigns spectral contribution ratios for the

assigned hyperfine fields for the θ-Fe_7C_3 phase. Therefore, the hyperfine fields corresponding to the specific non-equivalent Fe sites cannot be definitively identified from the literature for the θ-Fe_7C_3 phase at the moment.

To conclude, the MAS hyperfine field assignments for the θ-Fe_7C_3 phase are uncertain for the time being. However, as based on both experimental and theoretical data, the possible field assignments for the expected five sites for the orthorhombic θ-Fe_7C_3 phase are: 22.9 ± 0.1 T twice, 18.5 ± 0.1 T and 16.3 ± 0.1 T, with the field 21.0 T being uncertain. The hyperfine field spectral contribution ratios corresponding to the non-equivalent Fe site ratios are unassigned.

The assigned hyperfine fields for MAS fingerprinting of the Fe carbides encountered in the FTS reaction research, as based on the experimental literature data, are summarized in the Table 4. Hyperfine fields based on theoretical calculations by Liu et al., are reproduced in the table for comparison.[153]

5.6. Formation of Fe Carbides

Fe carbides form by dissolution of carbon atoms into the interstitial spaces in the α-Fe lattice. The formation of the various Fe carbides is primarily dependent on the temperature where the α-Fe lattice is exposed to an available source of carbon atoms. Fe in Fe carbides has a valency state close to zero, as for example in the χ-Fe_5C_2 phase.[24]

Fe carbides can form from α-Fe by: i) gas phase carburization where e.g. the CO, either from pure CO or H_2:CO, acts as the C source;[57,59] ii) heat treating the pre-formed Fe carbides to interchange the carbide phases,[57,68,77] and iii) tempering pre-formed martensite (or austenite) resulting in Fe carbide precipitation.[142,161] The ε-Fe_3C, η-Fe_2C, χ-Fe_5C_2 and θ-Fe_3C phases form relatively easily from an α-Fe/martensite precursor with any of the listed methods, i.e. by varying the heat treatment or gas phase carburization temperature. The formation of the θ-Fe_7C_3 phase seems to be a more complex phenomenon, as based on the available literature. It will be discussed separately after the formation conditions of the more common Fe carbides.

The observation temperatures for the ε-Fe_3C, η-Fe_2C, χ-Fe_5C_2 and θ-Fe_3C phases from the literature are gathered with the following criteria: i) the reaction takes place from metallic, zero valency α-Fe, in order to decouple the Fe reduction from carburization effects, ii) reaction treatment time is reported, and iii) it is possible to re-evaluate the reported data to correspond to the nomenclature, as defined in Table 3 and Table 4. From criteria iii) follows that only MAS- and ED-based results are included to evaluate the presence of the ε-Fe_3C and η-Fe_2C phases. XRPD and Thermomagnetic (TM) data are also included for evaluating the χ-Fe_5C_2 and θ-Fe_3C phases' formation behaviour. The references to the studies used to collect the data points in Figure 11 are collected in Table 5.

The collected data points in Figure 11 refer to the experimental observations on the Fe carbides after respective Fe carbide forming treatment. Possibly coexisting phases of α-Fe, martensite or Fe oxides are excluded from the figure.

The expected observation temperatures and carbide-to-carbide transition temperatures for the Fe carbides with 5 h treatment time can be roughly estimated as (Figure 11):

$$\varepsilon\text{-Fe}_3\text{C}\ (100-265\,^\circ\text{C}) < \eta\text{-Fe}_2\text{C}\ (160-350\,^\circ\text{C}) <$$

$$\chi\text{-Fe}_5\text{C}_2\ (240-350\,^\circ\text{C}) < \theta\text{-Fe}_3\text{C}\ (310-600\,^\circ\text{C})$$

Table 4. Mössbauer Absorption Spectroscopy (MAS) hyperfine field assignments based on the experimental literature data. The hyperfine fields are compared to the theoretically calculated values for the Fe carbides observable in the Fischer-Tropsch Synthesis (FTS) reaction research.

Fe Carbide Phase	Space Group	Non-equivalent Fe Positions[a] Tot. Count	Rel. Ratio	Hyperfine Field (at room temperature) Experimental[b] [T]	Theoretical[c] [T]
ε-Fe_3C	Hexagonal, $P6_322$ (182)	1	1	24.5 ± 0.8	N/A
η-Fe_2C	Orthorhombic, Pnnm (58)	1	1	17.2 ± 0.3	18.0[d]
χ-Fe_5C_2	Monoclinic, C2/c (15)	3	2	21.4 ± 0.3	23.7
			2	18.1 ± 0.4	20.9
			1	10.9 ± 0.9	14.0
θ-Fe_3C	Orthorhombic, Pnma (62)	2	(2)	20.8 ± 0.3	24.4
			(1)	20.0 ± 0.3	23.7
			Avg.[e]	20.8 ± 0.5	
θ-Fe_7C_3	Orthorhombic, Pnma (62)	5	(2)	22.9 ± 0.1	22.9
			(2)	-	22.9
			(1)	18.5 ± 0.1	18.7
			(1)	16.3 ± 0.1	17.4
			(1)	(21.0)[f]	19.9

[a] Determined on the basis of the crystal structures from authors in Table 3. The nominal relative ratios in parentheses () could not be conclusively assigned. [b] Mean hyperfine fields from the experimental literature data with their Standard Deviations (STDs). [c] Theoretical calculations by Liu et al. from reference [153]. No calculations were performed for the structure corresponding to Nagakura's ε-Fe_3C phase.[68] [d] Based on the unit cell of η-Fe_2C (#04-013-9510) from reference [135]. [e] Commonly, a single (averaged) hyperfine field is used for the θ-Fe_3C phase in the experimental literature data. [f] The assignment of hyperfine field 21.0 T for the θ-Fe_7C_3 phase is uncertain.

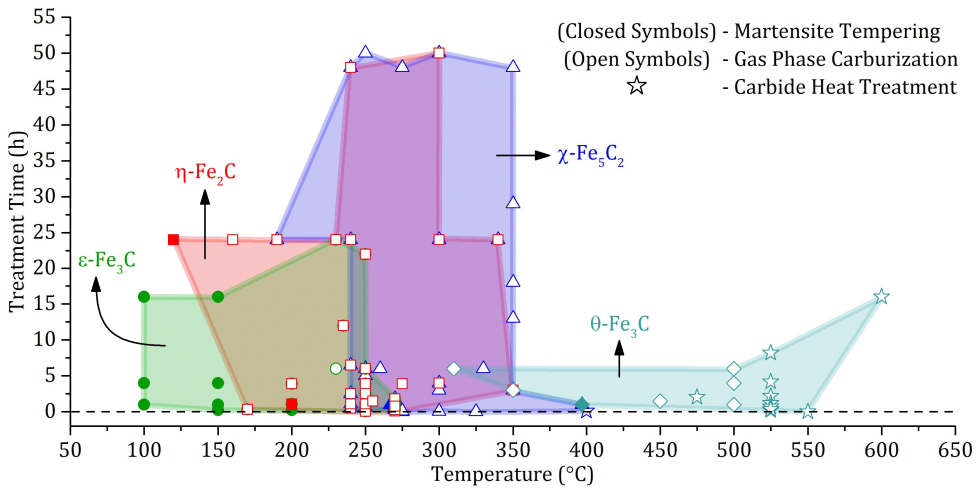

Figure 11. Collected observation regions (*solid fill*) of the Fe carbides as temperature versus treatment exposure time from experimental literature data. θ-Fe_7C_3 data points are excluded. Data points are collected according to the criteria presented in the text.

Table 5. The references to the experimental literature data for the Fe carbide formation observations, excluding the θ-Fe_7C_3 phase, and adhering to the criteria presented in the main text. The data points from the references are collected to the Figure 11.

Fe Carbide Phase	Characterization Techniques	Experiment Types	Reference Numbers
ε-Fe_3C	ED, MAS	- Gas phase carburization - Martensite tempering	[26,59,66,69,77,127,149,150,157,158]
η-Fe_2C	ED, MAS		[26,27,150,158,59,60,66,77,92,127,130,149]
χ-Fe_5C_2	ED, MAS, XRPD	- Gas phase carburization - Martensite tempering	[35,58,157,159,60,66,69,76,77,92,135,150]
θ-Fe_3C	ED, MAS, XRPD, TM	- Carbide heat treatment	[59,68,166,167]

ED = Electron Diffraction, MAS = Mössbauer Absorption Spectroscopy, XRPD = X-ray Powder Diffractometry, TM = Thermomagnetic.

These expectations on the Fe carbide thermal stabilities and the formation temperatures mainly compare well with the expectations presented by other authors.[57,68,133,142,161] This holds bearing in mind the unclear nomenclature in the literature regarding the "ε-carbides" i.e. the identification of the ε-Fe_3C and η-Fe_2C phases.

A good example on the behaviour of the ε-Fe_3C and η-Fe_2C phases is from a study by Boellaard, van der Kraan and Geus.[107] With the FTS reaction experiments at reaction temperatures between 200–275 °C, either increasing the reaction time or the temperature caused Fe carbide formation to shift from the ε-Fe_3C towards η-Fe_2C phase. Already at ~200 °C with ~1 h reaction time, the η-Fe_2C phase is the Fe carbide to form in larger quantities over the ε-Fe_3C phase. With further increasing the reaction time or temperature, the η-Fe_2C phase content increases.[107] In a martensite tempering study by Williamson, Nakazawa and Krauss,[132] at 200 °C the ε-Fe_3C phase (component M2 in their study) disappears if the tempering time is increased above 1 h. At temperatures < 150 °C, ε-Fe_3C is stable and is able to withstand longer tempering times.[132] In short, the ε-Fe_3C phase is the least stable Fe carbide that easily transforms to the η-Fe_2C phase, with increasing treatment time or temperature. Minor quantities of the ε-Fe_3C phase may nevertheless be observed with temperatures up to 250–270 °C.[58,65,107,155,162]

Within the temperature range of ~240–350 °C, both of the η-Fe_2C and χ-Fe_5C_2 phases may co-exist. For these carbides, the reaction exposure time seems to be less influential than in the case of relative formation of the ε-Fe_3C and η-Fe_2C phases. For at least up to 50 h in the FTS reaction at 300 °C, both the η-Fe_2C and χ-Fe_5C_2 phases can be observed, although at the higher temperatures the χ-Fe_5C_2 phase becomes the Fe carbide to form in higher quantities.[93] After a short 3 h FTS reaction, Niemantsverdriet et al. were able to observe low quantities of the η-Fe_2C phase even at 350 °C, while the χ-Fe_5C_2 and θ-Fe_3C phases were the major Fe carbide phases.[59] Also, after a 24 h FTS reaction at 340 °C, Wezendonk et al. observed a significant presence of the η-Fe_2C phase.[77]

Few catalyst composition properties are known to increase the stability of the ε-Fe_3C or η-Fe_2C phases (i.e., "ε-carbides") in relation to the χ-Fe_5C_2 phase. Addition of i) alkali, as at least if added as Na or K,[27,55,63,163] or ii) SiO_2 as an inert oxide,[60,72,155] to the Fe catalyst composition can stabilize the ε-Fe_3C and/or η-Fe_2C phase(s). Also, iii) smaller Fe particle size tends to favour the formation of the ε-Fe_3C and/or η-Fe_2C phases over the χ-Fe_5C_2.[59,155,164,165] Unfortunately, from the literature it is not possible to conclusively determine which of the "ε-carbides" i.e.

ε-Fe_3C and/or η-Fe_2C is stabilized, in relation to the mentioned catalyst composition properties.

Above the temperature of ~300–350 °C, the χ-Fe_5C_2 and θ-Fe_3C phases are the expected main Fe-carbide phases. The highest temperature stability for the χ-Fe_5C_2 phase included in this review, has been observed to be up to ~400 °C from a martensite tempering study.[161] Also, the χ-Fe_5C_2 phase has been observed after heat treating of preformed Fe carbides under vacuum at 400 °C for short periods of time (~0.1 h).[68] Above 350 °C, the preferred Fe carbide to form is θ-Fe_3C.[59,68,166,167]

From martensite tempering studies, Nagakura et al. have reported the formation of θ-Fe_3C after tempering martensitic steel at 267° for 1 h,[161] and Williamson, Nakazawa and Krauss after 250 °C for 5 h.[132] Both of these temperatures seem very low for θ-Fe_3C formation when comparing to the other literature data, and are excluded from the Figure 11.

Decomposition of the θ-Fe_3C phase into α-Fe and C under vacuum heat treatment may start already slowly at a temperature as low as 377 °C and becomes rapid at >527 °C as has been observed by Wood et al.[69] Nagakura in comparison observed that the θ-Fe_3C decomposition to α-Fe only started at ~600 °C under vacuum heat treatment.[68] The increase in the most thermally stable Fe carbide's (i.e., θ-Fe_3C) decomposition temperature has been explained by Podgurski et al. to be due to the formed Fe carbide oxidation shell.[71] The shell can retard the decomposition of the θ-Fe_3C core to α-Fe and C. The Fe carbides readily form a ~4–5 nm oxidation layer if any O is available for the oxidation reaction.[168]

As mentioned, the main Fe carbide phase determining factor is the temperature. For the gas phase carburization, factors such as H_2:CO ratio and reaction pressure, do not seem to play a significant role when the Fe carbides are formed from a zero valency α-Fe.

For example, with the FTS reaction at 250 °C with H_2:CO ratios of 1:1 (0.5 h),[58] 2:1 (1.1 h),[107] and 3:1 (0.66 h),[155] only the ε-Fe_3C (minor phase) and the η-Fe_2C (major phase) phases are observed along with differences in the extent of α-Fe carburization. At 270 °C after 0.66 h of FTS reaction with 10:1 H_2:CO, Tau et al. observed the formation of the χ-Fe_5C_2 phase in addition to the ε-Fe_3C and η-Fe_2C phases from α-Fe,[65] as would be expected on the basis of the reaction temperature (Figure 11). In a systematic study, Jung et al. have observed that an increasing H_2:CO ratio decreases the rate of carburization of α-Fe.[164] Despite the CO-rich atmosphere being favoured for the increased carburization rate, small amounts of (~1 %) H_2 can still aid the carburization more efficiently than CO by removing the surface O from CO dissociation,[29,52] as was also discussed in the previous sections. All in all, despite the changing H_2:CO ratios, the reaction temperature is still the determining factor for Fe carbide formation.

It is, however, worthy to emphasize again that when carburization with H_2:CO is done with *a Fe oxide* as the starting material *instead of α-Fe*, the Fe carbide formation is dependent on the simultaneous Fe reduction behaviour.[63,66,78,170,171] This can cause perceived deviations from the formation regions in Figure 11.

The effect of the overall reaction pressure under which the α-Fe phase is carburized from the gas phase is somewhat unclear from the literature, as systematic studies are lacking. It seems, however, that the increased pressure does not change the expected order of the Fe carbide formation, again, when *the carburization is done from the α-Fe phase.* Amelse et al. performed 300 °C FTS reaction (H_2:CO 3:1) for 24 h atmospheric pressure,[162] and Jiang et al. 300 °C FTS reaction (H_2:CO 1:1) at 10 bar pressure for 50 h.[93] In both studies, only the η-Fe_2C and χ-Fe_5C_2 phases were observed as the Fe carbides. After 30 bar FTS reaction (H_2:CO 2:1) for 0.3 h at 170 °C, Xu et al. observed only the ε-Fe_3C and η-Fe_2C phases as the Fe carbides.[154] With 23 bar FTS reaction (H_2:CO 3:2) at 235 °C for 12 h, only ε-Fe_3C and η-Fe_2C phases were present in a study by Wang et al.,[165] which is a quantification result comparable to 1.03 bar FTS reaction (3.9 h, 250 °C, H_2:CO 2:1) by Boellaard, van der Kraan and Geus.[107]

In each of the mentioned studies, the Fe carbide formation follows the expectations from the reaction temperature regardless of the applied reaction pressure. As noted by Xu et al., the elevated pressure only seems to increase the rate of carburization from α-Fe (see Supplementary Figure 2, in their study).[154] The formed Fe carbide phases, however, are not affected.

Finally, it is important to note that the formation of the θ-Fe_7C_3 phase is a special case, as it does not follow the temperature formation regions, presented in Figure 11. In literature, the θ-Fe_7C_3 phase is either observed to form at extreme conditions, such as at 60 kbar with >1100 °C from a mixture of graphite and α-Fe,[172] or via laser pyrolysis of $Fe(CO)_5$ under $C_2H_{2/4}$.[157,160,173]

A more interesting case for the FTS reaction related discussion in the realm of θ-Fe_7C_3 formation is observed in a study by Tajima and Hirano, where Ba-promoted Fe_3O_4 was carburized with pure CO at unspecified reaction pressure.[174] Within the temperature range of 300–375 °C, the Ba-Fe_3O_4 carburized into a mixture of the χ-Fe_5C_2 and θ-Fe_7C_3 phases.[174] Without Ba, only the χ-Fe_5C_2 phase was formed within the same temperature range from the unpromoted Fe_3O_4.[174,175] In a single crystal ED study of the θ-Fe_7C_3 phase by Audier, Bowen and Jones, single crystals of the θ-Fe_7C_3 phase were formed by carburizing the α-Fe phase under 3:1 CO:CO_2 at 500 °C.[148] As the carburization to, at least some amounts of, the θ-Fe_7C_3 phase took place without Ba or a Fe oxide, perhaps, the CO_2 might play a role in facilitating the formation of the θ-Fe_7C_3 phase. The θ-Fe_7C_3 phase has also been observed in catalysts extracted from industrial FTS reactors after long reaction times at high-pressure.[1]

A mechanical synthesis route for the θ-Fe_7C_3 phase has been attempted by Barinov, Tsurin and Surikov.[176] The route has more likely to have only formed the χ-Fe_5C_2 phase,[156] rather than any observable quantities of the θ-Fe_7C_3 phase.

Regarding the θ-Fe_7C_3 phase thermal stability, a heat treatment of the θ-Fe_7C_3 phase under He leads to the phase's decomposition, with decomposition temperature depending on the O atom impurity content in the θ-Fe_7C_3 crystal lattice.[173] High O atom impurity content causes the θ-Fe_7C_3 phase to decompose to Fe oxides and α-Fe between 300–400 °C. O atom

free θ-Fe_7C_3 phase can survive up to ~400–500 °C before decomposing directly to α-Fe and C atoms.[173]

To conclude, the formation of the θ-Fe_7C_3 phase does not follow the same route as for the ε-Fe_3C, η-Fe_2C, χ-Fe_5C_2 or θ-Fe_3C phases, but might have its own formation route. Nevertheless, θ-Fe_7C_3 phase formation is possible under relatively mild and FTS reaction relevant conditions, although more systematic research is needed on its formation specifics.

7. Summary and Outlook

Within this review article, the possible "C pathways" for C from CO and the associated chemical reactions in Fe-based Fischer-Tropsch Synthesis (FTS) were reviewed. Especially, effects from Na–S promotion were discussed. Furthermore, Fe carbides, which are considered to be the FTS active Fe phases, often have an unclear identification and their formation conditions were critically assessed based on the existing literature.

The following pathways can be active in Fe-based FTS reaction: *C from CO dissociation* can react i) with α-Fe to form Fe carbides, ii) with H from H_2 to form hydrocarbons, iii) with another C to form inactive carbon. *Without CO dissociation*, CO may iv) reduce Fe_xO_y or v) react via the WGS reaction with both pathways converting CO to CO_2. As catalyst deactivation pathways: the Fe_xC phases may re-oxidize to Fe_3O_4 under FTS reaction conditions if the local H_2O:H_2 or CO_2:CO ratios become too high. The Boudouard reaction as pathway iii) results in hindered reactant access to the catalysts surface and catalyst fragmentation. Modifying the process conditions and/or the catalyst compositions can be used as ways to modify the Fe-based FTS hydrocarbon and C pathway selectivities. Input H_2:CO ratio, reaction temperature and reactor space velocity are the main process parameters for modifying the α-value or olefin content of the FTS reaction produced hydrocarbons.

Addition of alkali individually increases the α-value and olefin content in FTS-synthesized hydrocarbons, while the individual addition of S does the opposite. Addition of combined alkali-S in the molar ratio of ≈2:1 increases the α-value less than with alkali only addition, and as an unique alkali-S promotion feature, decreases the CH_4 selectivity to a value lower than expected from the Anderson-Schulz-Flory (ASF) distribution. Also, the olefin content increases with the alkali-S addition akin to alkali-only addition. Possibly, S replaces O as the alkali counter-ion changing the chemical promoter compound binding on the Fe_xC surface, thereby affecting the promotion effects by alkali-S. On the C pathways, however, added alkali increases the inactive carbon deposition and WGS reactions, thereby decreasing the CO conversion towards hydrocarbon products. Unfortunately, the effect of individual S on the C pathways is still unclear. An increased CO_2 selectivity suggests an increased inactive carbon formation and/or WGS C pathways for alkali-S promoted catalysts – effects akin to alkali-only addition.

In this work, we also have identified the Fe carbides encountered in FTS research and assigned them with proper nomenclature and formation temperatures as:

- hexagonal ε-Fe_3C *$P6_322$* (182), (100–265 °C),
- orthorhombic η-Fe_2C *Pnnm* (58), (160–340 °C),
- monoclinic χ-Fe_5C_2 *C2/c* (15) (the Hägg carbide), (240–350 °C)
- orthorhombic θ-Fe_3C *Pnma* (62) (cementite), (310–600 °C),
- orthorhombic θ-Fe_7C_3 *Pnma* (62) (the Eckström-Adcock carbide).

The Mössbauer Absorption Spectroscopy (MAS) hyperfine fields were assigned for the carbides following the established nomenclature.

For further research, the exact effects of the different FTS active Fe carbides on the C pathways are still unclear. Determination of these effects has been hindered in the past by the imprecise and unclear Fe carbide nomenclature between different studies and characterization techniques. More precise understanding on the Fe carbide properties might offer an additional tool for altering the C pathways and overall C efficiency towards the hydrocarbon synthesis.

Acknowledgements

This research received funding from the Dutch Research Council (NWO) in the framework of the TASC Technology Area "Syngas, a Switch to Flexible New feedstock for the Chemical Industry (TA-Syngas)". Dow Chemicals and Johnson-Matthey are also acknowledged for their funding. Achim Iulian Dugulan (Delft University of Technology) is acknowledged for discussion on the MAS literature, while Pierre-Francois M. Vittoz (Universiteit Utrecht) for translation and discussion of reference [133].

Conflict of Interest

The authors declare no conflict of interest.

Keywords: Fischer-Tropsch Synthesis · Process Conditions · Na–S Promotion · Iron Carbides · Mössbauer Absorption Spectroscopy

[1] M. E. Dry, in *Catal. Sci. Technol.* (Eds.: J. R. Anderson, M. Boudart), Springer-Verlag, Berlin, **1981**, pp. 159–256.
[2] A. de Klerk, *Fischer-Tropsch Refining*, Wiley-VCH, Weinheim, **2011**.
[3] M. E. Dry, *Catal. Today* **2002**, *71*, 227–241.
[4] P. M. Maitlis, A. de Klerk, *Greener Fischer-Tropsch Processes for Fuels and Feedstocks*, Wiley-VCH, Weinheim, **2013**.
[5] A. de Klerk, in *Synth. Liq. Prod. Refin.* (Eds.: A. de Klerk, D. King), American Chemical Society, Washington, DC, **2011**, pp. 215–235.
[6] M. E. Dry, *Appl. Catal. A* **1999**, *189*, 185–190.
[7] H. M. Torres Galvis, K. P. de Jong, *ACS Catal.* **2013**, *3*, 2130–2149.
[8] Z. Zhang, J. Zhang, X. Wang, R. Si, J. Xu, Y. F. Han, *J. Catal.* **2018**, *365*, 71–85.
[9] A. H. Nasser, L. Guo, H. Elnaggar, Y. Wang, X. Guo, A. Abdelmoneim, N. Tsubaki, *RSC Adv.* **2018**, *8*, 14854–14863.
[10] M. G. A. Cruz, M. Bastos-Neto, A. C. Oliveira, J. M. Filho, J. M. Soares, E. Rodríguez-Castellón, F. A. N. Fernandes, *Appl. Catal. A* **2015**, *495*, 72–83.
[11] J. A. Díaz, A. Romero, A. M. García-Minguillán, A. Giroir-Fendler, J. L. Valverde, *Fuel Process. Technol.* **2015**, *138*, 455–462.
[12] X. Duan, D. Wang, G. Qian, J. C. Walmsley, A. Holmen, D. Chen, X. Zhou, *J. Energy Chem.* **2016**, *25*, 311–317.

[13] Z. Ma, C. Zhou, D. Wang, Y. Wang, W. He, Y. Tan, Q. Liu, *J. Catal.* **2019**, *378*, 209–219.
[14] D. Wang, J. Ji, B. Chen, W. Chen, G. Qian, X. Duan, X. Zhou, A. Holmen, D. Chen, J. C. Walmsley, *AIChE J.* **2017**, *63*, 154–161.
[15] H. Wang, S. Huang, J. Wang, Q. Zhao, Y. Wang, Y. Wang, X. Ma, *ChemCatChem* **2019**, *11*, 3220–3226.
[16] Y. Wei, D. Luo, C. Zhang, J. Liu, Y. He, X. Wen, Y. Yang, Y. Li, *Catal. Sci. Technol.* **2018**, *8*, 2883–2893.
[17] Z. Yang, M. Luo, Q. Liu, B. Shi, *Catal. Lett.* **2020**, DOI 10.1007/s10562-020-03147–6.
[18] M. A. Vannice, *J. Catal.* **1975**, *37*, 449–461.
[19] A. Mittasch, C. Schneider, *Producing Compounds Containing Carbon and Hydrogen*, **1916**, US1201850 A.
[20] J. Y. Johnson, *Improvements in the Manufacture and Production of Unsaturated Hydrocarbons of Low Boiling Point*, **1929**, GB322284A.
[21] R. Crous, T. C. Bromfield, S. Booyens, *Olefin Selective FT Catalyst Composition and Preparation Thereof*, **2010**, WO2010066386A1.
[22] G. F. Botes, T. C. Bromfield, R. L. J. Coetzer, R. Crous, P. Gibson, A. C. Ferreira, *Catal. Today* **2016**, *275*, 40–48.
[23] H. M. Torres Galvis, J. H. Bitter, C. B. Khare, M. Ruitenbeek, A. I. Dugulan, K. P. de Jong, *Science* **2012**, *335*, 835–838.
[24] J. Xie, J. Yang, A. I. Dugulan, A. Holmen, D. Chen, K. P. De Jong, M. J. Louwerse, *ACS Catal.* **2016**, *6*, 3147–3157.
[25] E. de Smit, B. M. Weckhuysen, *Chem. Soc. Rev.* **2008**, *37*, 2758–2781.
[26] G. P. van der Laan, A. A. C. M. Beenackers, *Catal. Rev.* **1999**, *41*, 255–318.
[27] R. Dictor, A. T. Bell, *J. Catal.* **1986**, *97*, 121–136.
[28] B. H. Davis, *Catal. Today* **2009**, *141*, 25–33.
[29] S. Krishnamoorthy, A. Li, E. Iglesia, *Catal. Lett.* **2002**, *80*, 77–86.
[30] J. W. Niemantsverdriet, A. M. van der Kraan, *J. Catal.* **1981**, *72*, 385–388.
[31] T. Riedel, H. Schulz, G. Schaub, K.-W. Jun, J.-S. Hwang, K.-W. Lee, *Top. Catal.* **2003**, *26*, 41–54.
[32] C. Rhodes, G. J. Hutchings, A. M. Ward, *Catal. Today* **1995**, *23*, 43–58.
[33] C. Ratnasamy, J. P. Wagner, *Catal. Rev.* **2009**, *51*, 325–440.
[34] W. Ngantsoue-Hoc, Y. Zhang, R. J. O'Brien, M. Luo, B. H. Davis, *Appl. Catal. A* **2002**, *236*, 77–89.
[35] A. P. Raje, R. J. O'Brien, B. H. Davis, *J. Catal.* **1998**, *180*, 36–43.
[36] M. Luo, B. H. Davis, *Appl. Catal. A* **2003**, *246*, 171–181.
[37] S. Chianese, J. Loipersböck, M. Malits, R. Rauch, H. Hofbauer, A. Molino, D. Musmarra, *Fuel Process. Technol.* **2015**, *132*, 39–48.
[38] N. Fischer, R. Henkel, B. Hettel, M. Iglesias, G. Schaub, M. Claeys, *Catal. Lett.* **2016**, *146*, 509–517.
[39] W. Ning, N. Koizumi, M. Yamada, *Energy and Fuels* **2009**, *23*, 4696–4700.
[40] M. Martinelli, C. G. Visconti, L. Lietti, P. Forzatti, C. Bassano, P. Deiana, *Catal. Today* **2014**, *228*, 77–88.
[41] C. H. Bartholomew, *Appl. Catal. A* **2001**, *212*, 17–60.
[42] M. E. Dry, T. Shingles, C. S. van H Botha, *J. Catal.* **1970**, *17*, 341–346.
[43] M. E. Dry, T. Shingles, L. J. Boshoff, C. S. van H Botha, *J. Catal.* **1970**, *17*, 347–354.
[44] E. M. Cohn, E. H. Bean, M. Mentser, L. J. E. Hofer, A. Pontello, W. C. Peebles, K. H. Jack, *J. Appl. Chem.* **1955**, *5*, 418–425.
[45] T. F. Berry, R. N. Ames, R. B. Snow, *J. Am. Ceram. Soc.* **1956**, *39*, 308–318.
[46] T. Herranz, S. Rojas, F. J. Pérez-Alonso, M. Ojeda, P. Terreros, J. L. G. Fierro, *J. Catal.* **2006**, *243*, 199–211.
[47] I. Alstrup, M. T. Tavares, C. A. Bernardo, O. Sørensen, J. R. Rostrup-Nielsen, *Mater. Corros.* **1998**, *49*, 367–372.
[48] P. E. Nolan, D. C. Lynch, A. H. Cutler, *Carbon* **1994**, *32*, 477–483.
[49] S. Mazzucco, Y. Wang, M. Tanase, M. Picher, K. Li, Z. Wu, S. Irle, R. Sharma, *J. Catal.* **2014**, *319*, 54–60.
[50] E. T. Turkdogan, J. V. Vinters, *Metall. Trans.* **1974**, *5*, 11–19.
[51] R. G. Olsson, E. T. Turkdogan, *Metall. Trans.* **1974**, *5*, 21–26.
[52] H. Arakawa, A. T. Bell, *Ind. Eng. Chem. Process Des. Dev.* **1983**, *22*, 97–103.
[53] A. C. J. Koeken, H. M. Torres Galvis, T. Davidian, M. Ruitenbeek, K. P. de Jong, *Angew. Chem. Int. Ed.* **2012**, *51*, 7190–7193; *Angew. Chem.* **2012**, *124*, 7302–7305.
[54] V. R. R. Pendyala, U. M. Graham, G. Jacobs, H. H. Hamdeh, B. H. Davis, *ChemCatChem* **2014**, *6*, 1952–1960.
[55] V. R. R. Pendyala, U. M. Graham, G. Jacobs, H. H. Hamdeh, B. H. Davis, *Catal. Lett.* **2014**, *144*, 1704–1716.
[56] J. F. Shultz, M. Abelson, K. C. Stein, R. B. Anderson, *J. Phys. Chem.* **1959**, *63*, 496–500.
[57] L. J. E. Hofer, *Nature of the Carbides of Iron*, **1966**.
[58] M. Pijolat, V. Perrichon, P. Bussière, *J. Catal.* **1987**, *107*, 82–91.
[59] J. W. Niemantsverdriet, A. M. van der Kraan, W. L. van Dijk, H. S. van der Baan, *J. Phys. Chem.* **1980**, *84*, 3363–3370.
[60] G. Le Caër, J. M. Dubois, M. Pijolat, V. Perrichon, P. Bussière, *J. Phys. Chem.* **1982**, *86*, 4799–4808.
[61] L. J. E. Hofer, E. M. Cohn, W. C. Peebles, *J. Am. Chem. Soc.* **1949**, *71*, 189–195.
[62] R. J. O'Brien, L. Xu, R. L. Spicer, B. H. Davis, *Energy Fuels* **1996**, *10*, 921–926.
[63] R. J. O'Brien, L. Xu, D. R. Milburn, Y.-X. Li, K. J. Klabunde, B. H. Davis, *Top. Catal.* **1995**, *2*, 1–15.
[64] W. Ning, N. Koizumi, H. Chang, T. Mochizuki, T. Itoh, M. Yamada, *Appl. Catal. A* **2006**, *312*, 35–44.
[65] L. M. Tau, S. Borcar, D. Bianchi, C. O. Bennett, *J. Catal.* **1984**, *87*, 36–54.
[66] E. de Smit, F. Cinquini, A. M. Beale, O. V. Safonova, W. van Beek, P. Sautet, B. M. Weckhuysen, *J. Am. Chem. Soc.* **2010**, *132*, 14928–14941.
[67] W. K. Jozwiak, E. Kaczmarek, T. P. Maniecki, W. Ignaczak, W. Maniukiewicz, *Appl. Catal. A* **2007**, *326*, 17–27.
[68] S. Nagakura, *J. Phys. Soc. Jpn.* **1959**, *14*, 186–195.
[69] I. G. Wood, L. Vočadlo, K. S. Knight, D. P. Dobson, W. G. Marshall, G. D. Price, J. Brodholt, *J. Appl. Crystallogr.* **2004**, *37*, 82–90.
[70] Y. Jin, A. K. Datye, *J. Catal.* **2000**, *196*, 8–17.
[71] H. H. Podgurski, J. T. Kummer, T. W. DeWitt, P. H. Emmett, *J. Am. Chem. Soc.* **1950**, *72*, 5382–5388.
[72] R. P. Mogorosi, N. Fischer, M. Claeys, E. van Steen, *J. Catal.* **2012**, *289*, 140–150.
[73] J. van de Loosdrecht, G. F. Botes, I. M. Ciobica, A. C. Ferreira, P. Gibson, D. J. Moodley, A. M. Saib, J. L. Visagie, C. J. Weststrate, J. W. Niemantsverdriet, in *Compr. Inorg. Chem. II* (Eds.: J. Reedijk, K. Poeppelmeier), Elsevier, Amsterdam, **2013**, pp. 525–557.
[74] T. Ren-Yuan, Z. Su, W. Chengyu, L. Dongbai, L. Liwu, *J. Catal.* **1987**, *106*, 440–448.
[75] R. B. Anderson, L. J. E. Hofer, E. M. Cohn, B. Seligman, *J. Am. Chem. Soc.* **1951**, *73*, 944–946.
[76] J. F. Shultz, W. K. Hall, B. Seligman, R. B. Anderson, *J. Am. Chem. Soc.* **1955**, *77*, 213–221.
[77] T. A. Wezendonk, X. Sun, A. I. Dugulan, A. J. F. van Hoof, E. J. M. Hensen, F. Kapteijn, J. Gascon, *J. Catal.* **2018**, *362*, 106–117.
[78] D. B. Bukur, K. Okabe, M. P. Rosynek, C. P. Li, D. J. Wang, K. R. P. M. Rao, G. P. Huffman, *J. Catal.* **1995**, *155*, 353–365.
[79] A. P. Steynberg, R. L. Espinoza, B. Jager, A. C. Vosloo, *Appl. Catal. A* **1999**, *186*, 41–54.
[80] A. Sarkar, D. Seth, A. K. Dozier, J. K. Neathery, H. H. Hamdeh, B. H. Davis, *Catal. Lett.* **2007**, *117*, 1–17.
[81] M. E. Dry, G. J. Oosthuizen, *J. Catal.* **1968**, *11*, 18–24.
[82] R. B. Anderson, F. S. Karn, J. F. Shultz, *J. Catal.* **1965**, *4*, 56–63.
[83] J. F. Shultz, L. J. E. Hofer, F. S. Karn, R. B. Anderson, *J. Phys. Chem.* **1962**, *66*, 501–506.
[84] J.-D. Xu, Z.-Y. Chang, K.-T. Zhu, X.-F. Weng, W.-Z. Weng, Y.-P. Zheng, C.-J. Huang, H.-L. Wan, *Appl. Catal. A* **2016**, *514*, 103–113.
[85] M. A. San-Miguel, J. Oviedo, J. F. Sanz, in *Handb. Nanophysics Clust. Fulleres* (Ed.: K. D. Sattler), CRC Press, Boca Raton, **2017**, pp. 328–344.
[86] J. K. Nørskov, S. Holloway, N. D. Lang, *Surf. Sci.* **1984**, *137*, 65–78.
[87] R. J. Madon, H. Shaw, *Catal. Rev.* **1977**, *15*, 69–106.
[88] J. Benziger, R. J. Madix, *Surf. Sci.* **1980**, *94*, 119–153.
[89] J. K. Nørskov, F. Besenbacher, *J. Less-Common Met.* **1987**, *130*, 475–490.
[90] J. K. Nørskov, T. Bligaard, B. Hvolbæk, F. Abild-Pedersen, I. Chorkendorff, C. H. Christensen, *Chem. Soc. Rev.* **2008**, *37*, 2163.
[91] B. Todic, L. Nowicki, N. Nikacevic, D. B. Bukur, *Catal. Today* **2016**, *261*, 28–39.
[92] M. E. Dry, *J. Organomet. Chem.* **1989**, *372*, 117–127.
[93] F. Jiang, M. Zhang, B. Liu, Y. Xu, X. Liu, *Catal. Sci. Technol.* **2017**, *7*, 1245–1265.
[94] G. F. Botes, J. W. Niemantsverdriet, J. van de Loosdrecht, *Catal. Today* **2013**, *215*, 112–120.
[95] M. E. Dry, in *Stud. Surf. Sci. Catal. – Fischer-Tropsch Technol.* (Eds.: A. P. Steynberg, M. E. Dry), Elsevier B. V., Amsterdam, **2004**, pp. 196–257.
[96] H. M. Torres Galvis, A. C. J. Koeken, J. H. Bitter, T. Davidian, M. Ruitenbeek, A. I. Dugulan, K. P. de Jong, *J. Catal.* **2013**, *303*, 22–30.
[97] W. W. Myddleton, *Improvements Relating to the Catalytic Synthesis of Hydrocarbon Oils from Gaseous Mixtures of Carbon Monoxide and Hydrogen*, **1939**, GB509325 A.
[98] H. M. Torres Galvis, A. C. J. Koeken, J. H. Bitter, T. Davidian, M. Ruitenbeek, A. I. Dugulan, K. P. De Jong, *Catal. Today* **2013**, *215*, 95–102.

[99] E. T. Layng, *Synthesis of Hydrocarbons with Sulfur Containing Catalyst*, **1948**, US2446426 A.
[100] H. P. Bonzel, *Surf. Sci. Rep.* **1988**, *8*, 43–125.
[101] M. Kiskinova, in *New Trends CO Act.* (Ed.: L. Guczi), Elsevier, Amsterdam, **1991**, pp. 37–86.
[102] G. Ertl, S. B. Lee, M. Weiss, *Surf. Sci.* **1981**, *111*, L711–L715.
[103] V. Ponec, in *New Trends CO Act.* (Ed.: L. Guczi), Elsevier, Amsterdam, **1991**, pp. 117–157.
[104] H.-B. Zhang, G. L. Schrader, *J. Catal.* **1985**, *95*, 325–332.
[105] B. W. Krupay, Y. Amenomiya, *J. Catal.* **1981**, *67*, 362–370.
[106] Y. Amenomiya, G. Pleizier, *J. Catal.* **1982**, *76*, 345–353.
[107] E. Boellaard, A. M. van der Kraan, J. W. Geus, *Appl. Catal. A* **1996**, *147*, 229–245.
[108] J. Paul, *Nature* **1986**, *323*, 701–703.
[109] M. E. Dry, T. Shingles, L. J. Boshoff, G. J. Oosthuizen, *J. Catal.* **1969**, *15*, 190–199.
[110] D. B. Bukur, D. Mukesh, S. A. Patel, *Ind. Eng. Chem. Res.* **1990**, *29*, 194–204.
[111] L. Guczi, *New Trends CO Act.* **1991**, *64*, 350–380.
[112] K.-R. Hwang, C.-B. Lee, J.-S. Park, *J. Power Sources* **2011**, *196*, 1349–1352.
[113] C. H. Bartholomew, P. K. Agrawal, J. R. Katzer, in *Adv. Catal.* (Eds.: D. D. Eley, H. Pines, P. B. Weisz), Academic Press, New York, **1982**, pp. 135–242.
[114] R. A. Dalla Betta, A. G. Piken, M. Shelef, *J. Catal.* **1975**, *40*, 173–183.
[115] W. L. van Dijk, J. W. Niemantsverdriet, A. M. van dar Kraan, H. S. van der Baan, *Appl. Catal.* **1982**, *2*, 273–288.
[116] X. Zhou, J. Ji, D. Wang, X. Duan, G. Qian, D. Chen, X. Zhou, *Chem. Commun.* **2015**, *51*, 8853–8856.
[117] T. Li, Y. Yang, Z. Tao, H. Wan, X. An, C. Zhang, H. Xiang, Y. Li, *J. Nat. Gas Chem.* **2007**, *16*, 354–362.
[118] H. G. Stenger, C. N. Satterfield, *Ind. Eng. Chem. Process Des. Dev.* **1985**, *24*, 415–420.
[119] B. Wu, L. Bai, H. Xiang, Y.-W. Li, Z. Zhang, B. Zhong, *Fuel* **2004**, *83*, 205–212.
[120] T. C. Bromfield, N. J. Coville, *Appl. Catal. A* **1999**, *186*, 297–307.
[121] F. S. Karn, J. F. Schultz, R. E. Kelly, R. B. Anderson, *Ind. Eng. Chem. Prod. Res. Dev.* **1963**, *2*, 43–47.
[122] A. Sarkar, A. K. Dozier, U. M. Graham, G. Thomas, R. J. O'Brien, B. H. Davis, *Appl. Catal. A* **2007**, *326*, 55–64.
[123] W. Arabczyk, D. Moszyński, U. Narkiewicz, R. Pelka, M. Podsiadły, *Catal. Today* **2007**, *124*, 43–48.
[124] Y. Sun, L. Tao, T. You, C. Li, H. Shan, *Chem. Eng. J.* **2014**, *244*, 145–151.
[125] D. Moszyński, H. J. Grabke, A. Schneider, *Surf. Interface Anal.* **2002**, *34*, 380–383.
[126] R. Warringham, A. L. Davidson, P. B. Webb, R. P. Tooze, S. F. Parker, D. Lennon, *Catal. Today* **2020**, *339*, 32–39.
[127] J. Xie, H. M. Torres Galvis, A. C. J. Koeken, A. Kirilin, A. I. Dugulan, M. Ruitenbeek, K. P. de Jong, *ACS Catal.* **2016**, *6*, 4017–4024.
[128] K. Momma, F. Izumi, *J. Appl. Crystallogr.* **2011**, *44*, 1272–1276.
[129] M. J. Duggin, L. J. E. Hofer, *Nature* **1966**, *212*, 248–248.
[130] K. H. Jack, S. Wild, *Nature* **1966**, *212*, 248–250.
[131] J. B. Butt, *Catal. Lett.* **1990**, *7*, 61–82.
[132] D. L. Williamson, K. Nakazawa, G. Krauss, *Metall. Trans. A* **1979**, *10*, 1351–1363.
[133] M. Dirand, L. Afqir, *Acta Metall.* **1983**, *31*, 1089–1107.
[134] G. H. Barton, B. Gale, *Acta Crystallogr.* **1964**, *17*, 1460–1462.
[135] Y. Hirotsu, S. Nagakura, *Acta Metall.* **1972**, *20*, 645–655.
[136] Y. Hirotsu, S. Nagakura, *Trans. Japan Inst. Met.* **1974**, *15*, 129–134.
[137] R. M. Stanfield, W. N. Delgass, *J. Catal.* **1981**, *72*, 37–50.
[138] G. Hägg, *Zeitschrift für Krist. – Cryst. Mater.* **1934**, *89*, 92–94.
[139] J. J. Retief, *Powder Diffr.* **1999**, *14*, 130–132.
[140] H. E. du Plessis, J. P. R. de Villiers, G. J. Kruger, A. Steuwer, M. Brunelli, *J. Synchrotron Radiat.* **2011**, *18*, 266–271.
[141] A. Leineweber, S. Shang, Z.-K. Liu, M. Widenmeyer, R. Niewa, *Zeitschrift für Krist.* **2012**, *227*, 207–220.
[142] L. J. E. Hofer, E. M. Cohn, *Nature* **1951**, *167*, 977–978.
[143] E. J. Fasiska, G. A. Jeffrey, *Acta Crystallogr.* **1965**, *19*, 463–471.
[144] Crystallography Open Database, "Open-access collection of crystal structures," can be found under http://www.crystallography.net/cod/, **2018**.
[145] H. C. Eckstrom, W. A. Adcock, *J. Am. Chem. Soc.* **1950**, *72*, 1042–1043.
[146] F. H. Herbstein, J. A. Snyman, *Inorg. Chem.* **1964**, *3*, 894–896.
[147] R. Fruchart, J. P. Senateur, J. P. Bouchaud, A. Michel, *Bull. Soc. Chim. Fr.* **1965**, *2*, 392.
[148] M. Audier, P. Bowen, W. Jones, *J. Cryst. Growth* **1983**, *63*, 125–134.
[149] U. R. Kattner, *J. Phase Equilib. Diffus.* **2013**, *34*, 437–437.
[150] O. A. Pringle, G. J. Long, in *Mössbauer Spectrosc. Appl. to Inorg. Chem.* (Eds.: G. J. Long, F. Grandjean), Springer, Boston, **1989**, p. 644.
[151] J. M. Dubois, G. Le Caër, *Acta Metall.* **1977**, *25*, 609–618.
[152] J. Foct, J. P. Senateur, J. M. Dubois, G. Le Caër, *Le J. Phys. Colloq.* **1979**, *40*, 647–649.
[153] X.-W. Liu, S. Zhao, Y. Meng, Q. Peng, A. K. Dearden, C.-F. Huo, Y. Yang, Y.-W. Li, X.-D. Wen, *Sci. Rep.* **2016**, *6*, 26184.
[154] K. Xu, B. Sun, J. Lin, W. Wen, Y. Pei, S. Yan, M. Qiao, X. Zhang, B. Zong, *Nat. Commun.* **2014**, *5*, 5783.
[155] G. B. Raupp, W. N. Delgass, *J. Catal.* **1979**, *58*, 348–360.
[156] V. A. Barinov, A. V. Protasov, V. T. Surikov, *Phys. Met. Metallogr.* **2015**, *116*, 791–801.
[157] X.-X. Bi, B. Ganguly, G. P. Huffman, F. E. Huggins, M. Endo, P. C. Eklund, *J. Mater. Res.* **1993**, *8*, 1666–1674.
[158] B. Kniep, A. Constantinescu, D. Niemeier, K. D. Becker, *Zeitschrift für Anorg. und Allg. Chemie* **2003**, *629*, 1795–1804.
[159] M. Ron, H. Shechter, A. A. Hirsch, S. Niedzwiedz, *Phys. Lett.* **1966**, *20*, 481–483.
[160] Y. Yamada, H. Yoshida, K. Kouno, Y. Kobayashi, *J. Phys. Conf. Ser.* **2010**, *217*, 012096.
[161] S. Nagakura, Y. Hirotsu, M. Kusunoki, T. Suzuki, Y. Nakamura, *Metall. Trans. A* **1983**, *14*, 1025–1031.
[162] J. A. Amelse, G. Grynkewich, J. B. Butt, L. H. Schwartz, *J. Phys. Chem.* **1981**, *85*, 2484–2488.
[163] X. An, B. Wu, H.-J. Wan, T.-Z. Li, Z.-C. Tao, H.-W. Xiang, Y.-W. Li, *Catal. Commun.* **2007**, *8*, 1957–1962.
[164] H. Jung, W. J. Thomson, *J. Catal.* **1992**, *134*, 654–667.
[165] P. Wang, W. Chen, F. Chiang, A. I. Dugulan, Y. Song, R. Pestman, K. Zhang, J. Yao, B. Feng, P. Miao, et al., *Sci. Adv.* **2018**, *4*, eaau2947.
[166] E. M. Cohn, L. J. E. Hofer, *J. Am. Chem. Soc.* **1950**, *72*, 4662–4664.
[167] J. F. Shultz, W. K. Hall, T. A. Dubs, R. B. Anderson, *J. Am. Chem. Soc.* **1956**, *78*, 282–285.
[168] S. Janbroers, J. N. Louwen, H. W. Zandbergen, P. J. Kooyman, *J. Catal.* **2009**, *268*, 235–242.
[169] J. A. Amelse, J. B. Butt, L. H. Schwartz, *J. Phys. Chem.* **1978**, *82*, 558–563.
[170] F. J. Berry, M. R. Smith, *J. Chem. Soc. Faraday Trans. 1 Phys. Chem. Condens. Phases* **1989**, *85*, 467–477.
[171] M. C. Ribeiro, G. Jacobs, B. H. Davis, D. C. Cronauer, A. J. Kropf, C. L. Marshall, *J. Phys. Chem. C* **2010**, *114*, 7895–7903.
[172] A. Tsuzuki, S. Sago, S.-I. Hirano, S. Naka, *J. Mater. Sci.* **1984**, *19*, 2513–2518.
[173] A. R. Sethuraman, *Nanostruct. Mater.* **1994**, *4*, 79–92.
[174] S. Tajima, S. Hirano, *Jpn. J. Appl. Phys.* **1990**, *29*, 662–668.
[175] S.-I. Hirano, S. Tajima, *J. Mater. Sci.* **1990**, *25*, 4457–4461.
[176] V. A. Barinov, V. A. Tsurin, V. T. Surikov, *Phys. Met. Metallogr.* **2010**, *110*, 474–484.

Manuscript received: March 28, 2020
Revised manuscript received: April 22, 2020
Accepted manuscript online: April 25, 2020
Version of record online: June 9, 2020